Deep Ionospheric Hole Created by Sudden Stratospheric Warming in the Nighttime Ionosphere

Goncharenko Larisa, P. (Orcid ID: 0000-0001-9031-7439)
Coster Anthea, J. (Orcid ID: 0000-0001-8980-6550)
Zhang Shun-Rong (Orcid ID: 0000-0002-1946-3166)
Benkevitch Leonid, V (Orcid ID: 0000-0001-7457-9084)
Harvey V., Lynn (Orcid ID: 0000-0002-7928-0804)
Reinisch Bodo, W (Orcid ID: 0000-0002-2158-6405)
Galkin Ivan, A (Orcid ID: 0000-0002-7286-8509)
Spraggs Mary (Orcid ID: 0000-0001-8336-8086)

Deep Ionospheric Hole Created by Sudden Stratospheric Warming in the Nighttime Ionosphere

L. P. Goncharenko[1], A. J. Coster[1], S.-R. Zhang[1], P. J. Erickson[1], L. Benkevitch[1], N. Aponte[2], V. L. Harvey[3], B. W. Reinisch[4], I. Galkin[5], M. Spraggs[6], A. Hernández-Espiet[7]

[1]MIT Haystack Observatory, Westford, MA, USA.

[2]Arecibo Observatory, Puerto Rico.

[3]Laboratory for Atmospheric and Space Physics, University of Colorado, Boulder, CO.

[4]Lowell Digisonde International, Lowell, MA, USA.

[5]University of Massachusetts Lowell, Lowell MA, USA.
[6]University of Wisconsin-Madison, Department of Atmospheric and Oceanic Sciences, USA.

[7]University of Puerto Rico at Mayagüez, Departamento de Matemáticas, 39 Mayagüez, Puerto Rico.

Corresponding author: Larisa Goncharenko (lpg@mit.edu)

Key Points:

- Impacts of sudden stratospheric warming on a nighttime ionosphere are studied
- SSWs affect the nighttime electron density, decreasing it by a factor of 2-4 in a large range of latitudes
- These effects are likely to be related to changes in thermospheric zonal wind

This is the author manuscript accepted for publication and has undergone full peer review but has not been through the copyediting, typesetting, pagination and proofreading process, which may lead to differences between this version and the Version of Record. Please cite this article as doi: 10.1029/2018JA025541

Abstract

Multiple observational studies have demonstrated large ionospheric variations during the daytime associated with sudden stratospheric warming (SSW) events, but only limited evidence of ionospheric disturbances during the night-time has been reported up to now. We focus on the American longitudinal sector with its extensive observational network of GPS receivers, four Digisondes located at low and middle latitudes, and the Arecibo and Millstone Hill incoherent scatter radars. The study focuses on a major SSW event of January 2013 to investigate large-scale disturbances in the nighttime ionosphere. We report a deep decrease in TEC that reaches a factor of 2-5 as compared to the background level and is observed between local midnight and local sunrise (6-12UT). This decrease is observed for several consecutive days in the range of latitudes from ~55^{o}S to ~45^{o}N. It is accompanied by a strong downward plasma motion and a significant decrease in ion temperature, as observed by both Arecibo and Millstone Hill radars. These results demonstrate that SSW events cause changes in the nighttime ionosphere that are even larger than in the daytime ionosphere. We discuss variations in electric field and *F*-region dynamics as possible drivers of this behavior, and suggest that thermospheric winds play a much larger role than previously thought.

Plain Language Summary

Large-scale meteorological disturbances like sudden stratospheric warmings are often used in research to illuminate a variety of mechanisms and processes that link different regions of the Earth's atmosphere across a wide range of altitudes and latitudes. Earlier studies have shown large and long-lasting anomalies caused by sudden stratospheric warmings in the Earth's daytime ionosphere. In this study, we show that in addition to the daytime changes, large changes also occur at night. In particular, major warming of January 2013 carved a deep hole in the nighttime ionosphere that extended through half the globe and decreased electron density by a factor of 2 to 4. These results suggest that strong disturbances occurred in the upper atmospheric wind system in a wide region from middle latitudes in the Northern Hemisphere to middle latitudes in the Southern Hemisphere. These results improve our understanding of reasons for very large day-to-day variations in the ionosphere and move us a step closer to improvements in space weather forecasting.

1 Introduction

The ionospheric research community often uses case studies like geomagnetic storms, high speed solar wind streams or X-ray flares to understand dominant physical processes that govern ionospheric behavior due to extreme solar forcing. In a complementary manner, recent studies of ionospheric behavior during sudden stratospheric warming (SSW) events have highlighted the significant role of meteorological forcing on the state of ionosphere (review Chau et al., 2012) and have initiated debates on the importance of different mechanisms connecting the troposphere, stratosphere, and ionosphere. As large ionospheric variations were reported in the low-latitude daytime ionosphere, most experimental and modeling studies focus on

understanding daytime ionospheric changes related to SSW. However, ionospheric disturbances during SSW at nighttime are also evident in earlier studies, although they were not emphasized at that time. Sumod et al. (2012) indicated that *foF2* obtained from the ionosonde at Trivandrum (Indian longitudinal sector, 8.5^{o}N, 77^{o}E, 0.5^{o}N dip latitude) during the minor SSW of January 2008 is significantly lower after sunset as compared to the background level. In the American longitudinal sector, large variations in the nighttime *foF2* during SSW of January 2009 can be seen at several locations in South America (Fagundes et al., 2015). de Paula et al., (2015) analyzed L-1 frequency scintillation data obtained at the southern crest of equatorial ionization anomaly in Brazil and concluded that scintillations are suppressed for extended period of times (up to several weeks) after SSW events.

To establish connections between ionospheric variations and changes in lower atmosphere conditions, an important first step is to determine an appropriate background ionosphere and rule out variations caused by known and regular factors (solar EUV radiation, magnetic and local solar time, season, and magnetic activity). The first studies of ionospheric effects of SSW used a multi-day averages prior to SSW to define the background ionosphere (e.g., Goncharenko et al., 2010). However, this approach has multiple deficiencies due to i) 27-day variation in solar flux, ii) the extended nature of ionospheric anomalies that can last for 3 weeks and longer (Goncharenko et al., 2010, 2013; Pedatella and Forbes, 2010), and iii) the seasonal changes due to direct heating/cooling by solar radiation and thermal heat conduction (Liu et al., 2014).

In this study, we investigate ionospheric variations observed during the SSW of January 2013 during nighttime hours in the American longitudinal sector using combined observations from GPS TEC receivers, several ionosondes, and the Millstone Hill and Arecibo incoherent scatter radars. Section 2 describes the instruments and data analysis procedure. To properly isolate SSW-associated ionospheric disturbances, we develop a set of local empirical models for each instrument used in this study. These models are discussed in section 3. Section 4 summarizes the stratospheric, solar flux, and geomagnetic variations during the winter 2012-2013 and presents detailed ionospheric observations. Section 5 examines nighttime data for other SSW events and discusses to what degree nighttime disturbances associated with SSW are repeatable.

2 Data sets and data analysis

2.1 GPS TEC

For this study we use global maps of ionospheric Total Electron Content derived from the world-wide network of GPS receivers (GPS-TEC) that are available from the year 2000 onwards (Rideout and Coster, 2006) in the Madrigal database system (http://madrigal.haystack.mit.edu/madrigal/). Continuous processed vertical TEC maps have 1^{o}x 1^{o} spatial resolution and 5 min temporal resolution, with 1-3 TEC unit uncertainty. We use GPS

TEC data for 15 available years (2000-2014) and include in the analysis Northern Hemisphere (NH) winter and spring periods (Nov 1 – Mar 31, 150 days per season). We focus on the American longitudinal sector, specifically, 75^{o}W, due to the best availability of GPS TEC receivers that allows detailed investigations of ionospheric behavior as a function of latitude. The number of receivers used in this study varies as a function of year, with approximately 1000 receivers available by the year 2014. Initial high-resolution data at 75^{o}W (+/-7.5^{o}) is averaged in 1-hour bins and preserves 1^{o} resolution in latitude, resulting in 15 years of continuous 150-day time series of TEC at latitudes 70^{o}S to 70^{o}N. Figure 1 presents an example TEC map resulting from 1-hour averaging and shows the locations of other instruments included in this study.

2.2 Ionosondes

Digisonde (Reinisch et al., 2009]) data are selected for three separate locations that are located close to incoherent scatter radars (ISR): Jicamarca, Peru (12^{o} S, 76.8^{o} W, ~2^{o}MLAT) co-located with the Jicamarca ISR; Ramey, Puerto Rico (18.5^{o} N, 67.1^{o} W, ~28^{o}MLAT, located close to the Arecibo ISR); and Westford, Massachusetts (Millstone) (42.6^{o} N, 71.5^{o} W, ~52^{o}MLAT) co-located with the Millstone ISR. In addition, data from the Port Stanley (51.6^{o} S, 57.9^{o} W, ~-42^{o}MLAT) ionosonde in the Falkland Islands are included in this study to provide wide latitudinal coverage. For direct comparison with GPS TEC and ISR data, we use the maximum electron density (*NmF2*) obtained from the GIRO database (Reinisch and Galkin, 2011). This study includes historic data available through GIRO, providing 18 winter periods for Millstone Hill (Nov 1996 – Mar 2014), 10 for Ramey (Nov 1999 – Mar 2014, data gaps in 2002-2003, 2007-2009), 20 for Jicamarca (Nov 1993 – Mar 2014), and 20 for Port Stanley (1995-2015), respectively.

2.3 Incoherent Scatter Radars

We use simultaneous observations from the Arecibo (18.3^{o}N, 66.8^{o}W) and Millstone Hill (42.6^{o}N, 71.5^{o}W) incoherent scatter radars to gain further understanding of variations in multiple ionospheric parameters within a broad height range. Both radars operated for extended period of time during January 2013 as a part of a coordinated campaign to collect data associated with the SSW. Both radars provide observations of electron density *Ne*, electron temperature *Te*, ion temperature *Ti*, and line-of-sight ion drift velocity *Vi* in the *E* and *F*-regions. For the purpose of this study we focus on the ionospheric *F*- region parameters.

3 Results

3.1. Background ionospheric behaviour

3.1.1. Empirical models of TEC and *NmF2*

To separate effects of meteorological or other types of forcing from known effects of solar, geomagnetic activity, and seasonal change, we have developed an empirical model of TEC

based on 15 years of data. Each spatial (75°W+/- 7.5°) and temporal (1 hour) bin was fit with a formula

$$TECm = TEC_o + b_1\, PF_{107} + b_2 PF_{107}^2 + b_3\, Ap_3 + b_4\, Ap_3^2 + b_5\, Ap_{3-3} + b_6 Ap_{3-6} + b_7 Ap_{3-9} + b_8 \sin\frac{2\pi\, DOY}{365} + b_9 \cos\frac{2\pi\, DOY}{365} + b_{10} \sin\frac{4\pi\, DOY}{365} + b_{11} \cos\frac{4\pi\, DOY}{365} + b_{12} PF_{107} \sin\frac{2\pi\, DOY}{365} + b_{13} PF_{107} \cos\frac{2\pi\, DOY}{365} \quad (1)$$

This formula includes a dependence on a solar flux proxy $PF_{107} = (F10.7 + F10.7_{81ave})$, where *F10.7* and $F10.7_{81ave}$ are solar flux for the previous day and 81-day average, respectively, a dependence on current and previous geomagnetic activity (terms with Ap_3, $Ap_{3\text{-}3}$, $Ap_{3\text{-}6}$, $Ap_{3\text{-}9}$, where Ap_3 is a current geomagnetic activity index, $Ap_{3\text{-}3}$ is geomagnetic activity during previous 3 hours, etc.), and a seasonal variation as a function of day of year (DOY). Terms with coefficients b_{12} and b_{13} represent cross-terms between solar flux and seasonal variations. Coefficients b_1-b_{13} are determined through a least square fit to available data. We note that for GPS TEC data such coefficients are obtained independently for every 1° in latitude and for every hour, thus avoiding potential artificial features that can be introduced by fitting with 24h, 12h, and 8hr tides. For ionosonde data, coefficients were obtained with 1-hour resolution for the Port Stanley location, and at 15-min resolution for the other locations. Higher temporal resolution enables the accurate description of NmF2 behavior during and after sunrise and sunset. Figure 2 shows *NmF2* observations for 120 < *F10.7* < 140 sfu and predictions by our empirical models for *F10.7* = 130 sfu conditions as a function of season and universal time (UT) for four different locations: Millstone Hill, Ramey, Jicamarca, and Port Stanley, representing winter mid- latitude ionosphere, low-latitude winter hemisphere ionosphere, magnetic equator summer hemisphere ionosphere, and summer mid-latitude ionosphere, respectively. The tickmarks in the figure correspond to the first day of the month. The seasonal variation is obtained using the data within +/- 15 days from the specified date. The models illustrate well such expected features as higher electron density and stronger semi-annual oscillation in the low-latitude ionosphere (Jicamarca and Ramey). All locations exhibit a mid-winter decrease in electron density. The magnitude and timing of this decrease varies with location, with significant differences in timing between the dayside (~12-24 UT) and nightside (~0-12 UT). Comparison between predictions of our TEC models and *NmF2* models and various data subsets (not shown here) shows mainly the same behavior in TEC and *NmF2* data, albeit that data/model differences are easier to distinguish in *NmF2*. This aspect is important for comparisons with physics-based models that have upper boundary of the order of several hundred kilometers.

Figure 3 illustrates the performance of the *NmF2* models with season and local time using such common metrics as Mean Absolute Percentage Error (MAPE, left) and Root Mean Square Error (RMSE, right). The MAPE is defined as:

$$MAPE = \frac{100}{n}\sum_{i=1}^{n}\left|\frac{NmF2_{data_i} - NmF2_{model_i}}{NmF2_{data_i}}\right|,$$

where $NmF2_{data_i}$ is the observed value and $NmF2_{model_i}$ is the predicted value. In figure 3, variations in MAPE and RMSE are calculated for data with 100 < *F10.7* < 150 and Ap < 80 to minimize errors associated with extreme conditions.

The daytime MAPE varies mostly within 13-17% at Millstone Hill and Ramey, increases to 20-25% at Jicamarca, and is even higher, at 25-30%, at Port Stanley. The nighttime MAPE is obviously higher due to the low electron density, but over Port Stanley the daytime MAPE remains higher than the nighttime MAPE. Of a particular interest to this study, increase in a nighttime MAPE is well pronounced at Millstone Hill and Jicamarca stations, while at Ramey increase in MAPE is observed in a more limited local time range, 7-10 UT and ~22-02 UT. Variations in RMSE (Figure 3, right panels) illustrate the performance of models in a manner complementary to MAPE and indicate that the largest RMSE are observed during the daytime hours and follow the seasonal variation in *NmF2* (compare to Figure 2). Overall, Figure 3 shows typical uncertainties of the empirical models that can be used to isolate ionospheric anomalies due to the different drivers.

Subtracting the empirical model prediction from the data produces residuals that cannot be directly driven by influences of seasonal change, solar activity, and geomagnetic activity, and contains the potential influence of meteorological origin. Analysis of the residuals does not show significant correlation with season or with indices of solar or geomagnetic activity (for geomagnetic storms weaker than Kp = 6+). The periods of geomagnetic disturbances with Kp > 6+ are relatively rare in these datasets, and the largest residuals are observed primarily during quiet geomagnetic conditions (Ap <= 5).

We note that inclusion of additional terms in the fit formula (1) does not significantly reduce residuals and does not change the results of this study. The main MAPE and RMSE seasonal features described above do not depend on a selected solar activity range, though in general MAPE is higher for lower solar activity, and RMSE is higher for higher solar activity. For TEC models (not shown here), seasonal and local time features in MAPE and RMSE are similar to those presented in Figure 3 for *NmF2* models, suggesting that these features are driven by the underlying ionospheric variability. The daytime MAPE values for TEC models are lower than for *NmF2* models and remain within 10-15% for 42^{o}N and 18^{o}N (close to Millstone Hill and Ramey locations) and within 6-10% for 12^{o}S (close to Jicamarca location). The nighttime MAPE values in TEC models are of the order of 15-20% at 42^{o}N, 20-25% at 18^{o}N, and 20-35% at 12^{o}S. Overall, we conclude that the local empirical models provide an accurate description of the mean state for various ionospheric features and can serve as the climatological specification of the ionosphere in the American longitudinal sector during the November-March period.

3.1.2. Empirical models of other ionospheric parameters

To isolate anomalous behavior in data obtained by incoherent scatter radars, we used empirical models of *Ne*, *Te*, *Ti*, and *Vi* built on multiple years of observations (Zhang et al., 2005). The Millstone Hill empirical model was originally developed in 2005 and included data

collected in 1976-2001. To improve the model's ability to reproduce ionospheric behavior due to solar-geophysical conditions, the Millstone Hill empirical model was updated with wintertime data (November – February) collected between 2002 and 2014. The Arecibo empirical model is based on data collected in 1970-2002.

3.2 Observations during SSW 2013

3.2.1 Stratospheric anomalies and geomagnetic situation

A long-lasting major sudden stratospheric warming (SSW) occurred in January 2013 during moderate-to-high solar activity conditions that peaked on January 6-8, 2013 and persisted for 3 weeks. An overview of anomalies in stratospheric parameters is given in Goncharenko et al. (2013) (see their Figure 1). This warming also coincided with a large variation in solar activity due to the 27-day periodicity, with solar flux *F10.7* index changing from ~104-110 sfu at the end of December 2012 to 174 sfu on January 10. Previous studies report large variations in the daytime ionosphere associated with SSW influences, with maximum changes occurring in mid-January 2013 (Goncharenko et al., 2013; Jonah et al., 2014). In addition, increased geomagnetic activity was observed on Jan 13 (Kp=4-) and Jan 17 (Kp=4), contributing to the complexity of ionospheric variations, as noted by Maute et al., (2015).

3.2.2. Analysis of ionospheric data

Here we present a subset of results from observations by different instruments, with a focus on the nighttime ionosphere. Figure 4 shows observations of TEC at 75^{o}W at 8UT (3LT) for several consecutive days in mid-January in comparison with our empirical TEC model described in section 3.1 (thick black line). Thick dash lines show 25th and 75th percentiles of all TEC data (1-hour bins) collected during similar season (DOY=350-410 or 16 Dec-14 Feb) and solar activity (*F10.7*=119-135). Thin dashed lines show 10th and 90th percentiles of TEC data for the same range of days and solar flux. We note that the data used in the calculation of percentiles includes periods of multiple SSW events and geomagnetic storms. For all latitudes, the empirical model lies within the boundaries presented by 25th and 75th percentiles. For the purpose of this study, we consider these boundaries as "usual" ionospheric behavior. The main feature of the average behavior is a gradual decrease in TEC from high latitudes in the Southern Hemisphere to high latitudes in the NH, which represents the expected seasonal summer-to-winter variation. In addition, two TEC peaks can be identified as superposed on the seasonal variation. One minor peak is centered at the equator and represents a northern crest of the equatorial ionization anomaly, while a second large peak is centered at ~30^{o}N and represents a post-midnight increase in electron density.

We define as "anomalous" behavior TEC observations as being either above the 75th percentile or below the 25th percentile. "Highly anomalous" behavior is defined as TEC values outside either the 90th or 10th percentiles. As Figure 4 shows with illustration for Jan 15-18, 2013, there are multiple days where the nighttime TEC was abnormally low in an extended range of latitudes, from ~55^{o}S to ~40^{o}N. The decrease in the observed TEC varies from a factor of ~2

in the low-latitude ionosphere to a factor of ~4 at 40°S. In addition, the mid-latitude peak in the nighttime TEC that was centered at ~30°N for average conditions, has moved to higher latitudes for all four cases, and is centered at ~36-39°N. Thus, the mid-latitude NH (~35-55°N) experiences a decrease or increase in TEC during this period that is predominantly driven by a latitudinal displacement of post-midnight increase in electron density.

Figure 5 presents the TEC anomaly on Jan 16, 2013 as a function of UT expressed as data-to-model ratio, TEC_{data}/TEC_{mod}. Deep depletion exceeding a factor of 3-4 of the background TEC level is observed throughout the local night hours (6-11 UT, 1-6 LT), with maximum depletion occurring deeper and earlier in the Southern Hemisphere (SH). We interpret a weakening of the depletion at ~10-20°S as being caused by the Equatorial Ionospheric Anomaly (EIA) superimposed on a general deep ionospheric depletion that extends from ~50°S to ~40°N. There is a clear latitudinal gradient in the timing of the TEC depletion, with the largest TEC decreases observed around ~8:30 UT at mid-latitudes in the SH, and at ~9:30-10:00 at mid-latitudes in the NH.

Ionosonde observations of *NmF2* at four locations close to 75°W are shown in Figure 6. We use every other day (Jan 14, 16, 18) to illustrate salient features of the observations. According to Fig. 6, Jicamarca and Ramey ionosondes observe the ionosphere well inside of the area of nighttime TEC depletion, while the Port Stanley and Millstone Hill ionosondes sample the ionosphere close to the latitudinal boundaries of this depletion. During the daytime (~12-24 UT), a deep negative anomaly at the magnetic Equator (Jicamarca) coincides with a large positive anomaly ~15° north of the EIA crest (Arecibo). This behavior is consistent with expectations of enhancement in the upward vertical drift (electric field) at the magnetic equator during SSW. The enhanced vertical drift will move plasma away from the equator and dramatically increase electron density in the EIA crests (e.g. Chau et al., 2010; Goncharenko et al., 2010a,b, 2013). At middle latitudes, however, ionospheric disturbances are more complex, with consistently large daytime increases in *NmF2* at the SH mid-latitude station (Port Stanley) and much smaller positive and negative disturbances at the NH mid-latitude station (Millstone Hill). Such variations are not expected to result from electric field disturbances at the magnetic equator, and are likely produced by disturbances in the thermospheric wind system. However, the nighttime (~0-12 UT) depletion in *NmF2* is observed in all four locations, albeit not every day in the northern mid-latitudes (Millstone Hill). For several hours per night *NmF2* at all four stations decreases to below the 25th percentile range and sometimes even below the 10th percentile range, indicating anomalously low electron density. We note that on January 18, 2013 the low-latitude F-region becomes strongly disturbed, with spread-F development between 8-11 UT, resulting in an *NmF2* data gap in Jicamarca data. An extremely low *NmF2* is observed on that night at the other three ionosondes, Port Stanley, Ramey and Millstone Hill, indicating that the area of anomalously low nighttime electron densities extends from mid-latitudes in the SH to mid-latitudes in the NH. The latitude of Millstone Hill presents the northern border of the affected area, with *NmF2* depletion reaching 42°N on some nights but not others, while the anomalously low *NmF2* (or the Spread-F) persists at lower latitudes for several nights.

An important aspect of these observations is that a later occurrence of deep depletion is observed at higher northern latitudes, as shown in Figures 5 and 6. Figures 7 and 8 highlight this aspect with observations of ionospheric parameters by Millstone Hill and Arecibo incoherent scatter radars, respectively. The left panels show electron density (*NEL*, log10), electron temperature (*Te*), ion temperature (*Ti*), and vertical drift velocity (*Vi*) for this level of solar flux and season as predicted by empirical models, while right panels show observations on January 18, 2013. Black lines indicate the time of local sunrise at ionospheric altitudes. A sharp, deep decrease in NEL develops over Millstone Hill before the local sunrise and is observed at ~9:30-12 UT; the electron density prior to that (0-9UT) and after (12-18 UT) is strongly increased in comparison with the empirical model predictions. The pre-sunrise to sunrise decrease in *NEL* is accompanied by an increase in electron temperature up to 500 K, which is anti-correlated with *NEL*. In addition, a strong decrease in ion temperature (up to 250 K and higher) is observed around sunrise, with particularly large cooling above 300 km altitude. Vertical drifts indicate complex variations, with predominantly downward ionospheric motion below 300 km which is 20-30 m/s stronger than average. At Arecibo (Figure 8), a similar deep decrease in NEL also develops prior to the local sunrise and is observed at 8:30-10:30 UT, e.g., 1-1.5 hours earlier than over Millstone Hill. In the same manner as for Millstone Hill, a sharp sunrise decrease in NEL is accompanied by NEL increases at night (0-7 UT) and during the daytime (15-18 UT), indicating that the same processes could be responsible for ionospheric variations at locations separated by 24 degrees in latitude. The electron temperature over Arecibo rises as much as 500-1000 K during this time period, while the downward vertical drift reaches 80-90 m/s, in contrast to ~10-15 m/s expected at this time. A decrease in ion temperature is also observed, but weaker than over mid-latitude and only at high altitudes, above ~400km.

3.3 Observations during other SSW events

Observations of large disturbances in the nighttime and sunrise ionosphere over extended latitude ranges during the major SSW of January 2013 raise the question: are there similar disturbances occurring in the nighttime during other SSW events? To answer this question, we examine GPS TEC data for Northern Hemisphere winters from 2008 to 2012, focusing on time periods when large daytime disturbances were previously reported (e.g. Chau et al., 2012; Goncharenko et al., 2010a,b). Due to the more sparse coverage of GPS receivers in earlier years, data quality does not always allow observations over an extended range of latitudes.

3.3.1 SSW of January 2008

A minor SSW event occurred in the end of January 2008 with a peak on January 23. Solar and geomagnetic activity was very low during this period. This event resulted in dramatic variations in the daytime equatorial vertical drift as seen at the Jicamarca observatory (Chau et al., 2009) and corresponding variations in the daytime TEC (Goncharenko et al., 2010b). Figure 9 (left panel) presents TEC data/model ratios at nighttime on January 28, 2008 to demonstrate nighttime variations. A broad area of decreased TEC is observed from southern mid-latitudes to

northern mid-latitudes, with a TEC increase at 0-5 UT and 0-10^{o}N related to variations in the EIA crest. This decrease is weaker than during the major SSW of January 2013 (up to a factor of 2) and covers a smaller span of latitudes, but the main features of the nighttime depletion are the same. Figure 10 presents *NmF2* observations by the Jicamarca ionosonde during the nighttime (0-12 UT, left panel) and daytime (12-24 UT, right panel) for several days. Daytime *NmF2* is strongly disturbed between 14-20 UT, decreasing to levels well below the 10th percentile for this level of solar flux (F10.7 = 69-75 sfu). During the nighttime, there is evidence of a decrease in *NmF2* between 0-4 UT, and Spread-F is observed between 4-10 UT.

3.3.2 SSW of January 2012

A minor SSW event in January 2012 began on January 10, peaked on January 19, 2012 and occurred during a period of medium solar activity (*F10.7* = 130-157 sfu). Ionospheric disturbances often maximize several days after the peak stratospheric disturbances. The interpretation of the ionospheric observations after the peak of this SSW event is complicated due to the superposition of several other geoeffective events: the M-class solar flare on January 19; the moderate geomagnetic storms on January 22-25; and a strong solar energetic particle precipitation event on January 23-30. Still, the SSW-associated disturbances can be isolated prior to the peak of the SSW. A decrease in TEC up to 50-60% of its expected value over a broad range of latitudes can be seen for several days prior the maximum in stratospheric temperature, as illustrated in Figure 9b (right).

4 Discussion

As the behaviour of the night-time ionosphere is strongly controlled by chemical composition and transport processes, detailed studies of observed night-time ionospheric disturbances help to test different hypotheses of coupling including vertical coupling between atmospheric layers, horizontal coupling between different latitudes, and coupling between ions and neutrals.

Large variations in nighttime electron density occur on the same dates (January 14-18, 2013) as large variations in daytime electron density (Figure 6). The timing of the responses suggests that a common mechanism may explain the observed disturbances. As multiple studies addressing daytime ionospheric variations during SSWs point to the importance of solar and lunar semidiurnal tides amplified by propagation through the SSW-modified middle atmosphere [Fuller-Rowell et al., 2010; McDonald et al., 2015; Pedatella and Liu, 2013], it is reasonable to assume that tidal modifications affect the nighttime ionosphere as well. Numerical simulations indicate that the bulk of the daytime ionospheric changes at low latitudes results from modification of the daytime eastward electric field that is generated by semidiurnal tidal winds in the lower thermosphere [e.g., Pedatella et al., 2014]. At nighttime, the electric field is mostly westward, producing downward vertical motion, and a semidiurnal perturbation in the electric field can produce multi-hour decreases in electron density. However, thermospheric wind

modification resulting from tidal changes can also play a very important role. Numerical simulations indicated the importance of the thermospheric neutral wind in creating ionospheric anomalies during SSWs (Pedatella et al., 2014, Pedatella and Maute, 2015). In this study, the later occurrence of a deep decrease in electron density at more northern latitudes (as compared to more southern latitudes), as well as the association of such a decrease with local sunrise, are not consistent with the electric field as a main mechanism responsible for ionospheric variations during the SSW.

Although both meridional and zonal components of thermospheric neutral wind could be disturbed during SSW (Miyoshi et al., 2015), our observations could indicate that the nighttime decrease in *Ne* is more likely related to variations in the *F*-region zonal winds, rather than meridional winds. It is well known that the thermospheric meridional wind is one of the efficient drivers of changes in ionospheric electron density, especially at middle latitudes, as it transports plasma up (or down) magnetic field lines to altitudes of lower (or higher) recombination rates. Analysis of sources of electron density variations during SSWs (Pedatella et al., 2014) indicates significant (of the order of 50 m/s) SSW perturbations in the thermospheric meridional wind that were attributed to upward propagating semidiurnal solar and lunar tides. However, these wind perturbations have different signs in different hemispheres and lead to different types of electron density perturbations in the NH vs. SH, and in the bottom-side ionosphere vs. topside ionosphere. A series of recent studies have demonstrated that, in addition to the meridional wind, zonal thermospheric wind can strongly affect ionospheric electron density due to effects of magnetic declination (Zhang et al., 2011, 2012). As magnetic declination is positive along the 70^{o}W longitude in the NH and typical pre-sunrise thermospheric wind is directed westward, vertical drift induced by this wind is directed downward. Enhancement in the westward perturbation that can be expected at low to middle latitudes according to numerical simulations (Liu et al., 2014), should further increase this downward drift. In addition, as magnetic declination varies with longitude, SSW-induced perturbations to the zonal wind could contribute to significant longitudinal differences in ionospheric effects reported by multiple authors (Bolaji et al., 2016; Goncharenko et al., 2013; Maute et al., 2015; Vieira et al., 2017].

Although this hypothesis about the importance of the zonal thermospheric wind needs further experimental and modeling support, it points to another possible mechanism for the connection between the middle atmosphere and ionosphere. Observed disturbances in *NEL*, *Te*, and *Vi* over a tropical location (Arecibo) are similar to disturbances over a mid-latitude location (Millstone Hill), but much stronger, consistent with the wide latitudinal area of depleted electron density depicted by the GPS TEC measurements (Figure 5). They can be explained in terms of combined influences of electric fields strongly disturbed by SSW-associated semidiurnal tides and thermospheric neutral wind.

A post-midnight increase in mid-latitude ionospheric electron density is a well-documented phenomenon (e.g., Chen et al., 2015; Farelo et al., 2002, and references therein). Different mechanisms were proposed to explain this phenomenon, including plasmaspheric flux

from the conjugate ionosphere (Evans, 1965), increased downward flux from the plasmasphere (e.g., Bailey et al., 1991; Jakowski and Forster 1995), and enhanced meridional neutral wind (Mikhailov et al., 2000). Our analysis of TEC data following several SSW events indicates that on average a post-midnight increase in electron density is very strong at 75^{o}W and maximizes at 30-33^{o}N (Figure 4), consistent with COSMIC observations (Chen et al., 2015). During the SSW of 2013, the latitudinal peak in the post-midnight density increase shifted poleward by ~5-7 degrees, leading to an increase in electron density and TEC at 40-50^{o}N on January 18, 2013 (Figure 4). Observations by the Millstone Hill incoherent scatter radar and ionosonde (42^{o}N) indicate that anomalously high electron density was observed on January 18 between 0-9 UT. However, plasma drift at altitudes above the *F*-region peak, which is typically directed downward varying between 10-20 m/s, was weaker than usual or even directed upward prior to ~7:00 UT, and became stronger and directed downward only after ~7:30 UT (Figure 7). Thus, the latitudinal variation of the night-time enhancement in TEC and prolonged increase in electron density at 42^{o}N support a hypothesis that a significant portion of this increase is driven by the thermospheric wind system and not by the downward flux from the plasmasphere.

Observations from ionosondes presented in this study suggest the development of Spread-F at times and latitudes of deep ionospheric TEC depletions. Although this study does not specifically address the association between SSWs and Spread-F, it points to a potential connection. de Paula et al. (2015) reported a weakening of GPS scintillations (S4 index) during several SSW events at a single low-latitude location, suggesting a decrease in small-scale ionospheric irregularities. Observations at multiple low-latitude locations during the 2006 SSW event did not report a similar decrease, although the study investigated large-scale irregularities (rate of change of TEC - ROT) (de Jesus et al., 2017). Frissell et al. (2016) concluded that at middle latitudes the occurrence of medium-scale traveling ionospheric disturbances (MSTIDs) is correlated with the strength of the stratospheric polar vortex, and MSTIDs are suppressed and reach a minimum 1-2 weeks after a weak polar vortex. Development of ionospheric irregularities and TIDs remains an open question for ionospheric research, with some studies support hypotheses of auroral and space weather sources, and other studies highlight sources related to tropospheric weather and gravity wave seeding. As the atmospheric wind system is strongly perturbed during SSW events over a large range of latitudes and altitudes, it is expected that such perturbations will modify gravity wave propagation conditions and thus affect ionospheric irregularities and TIDs. Further studies are required in order to get a comprehensive understanding of how ionospheric irregularities respond to changing neutral atmospheric dynamics.

5 Summary and Conclusions

We use observations that utilize three different techniques (GPS, Digisondes, and incoherent scatter radars) to examine the behavior of the nighttime ionosphere during the major SSW event of 2012-2013, and test the consistency of the results using minor SSWs of 2008 and 2012. Main results of this study are summarized as follows:

1. To properly separate SSW effects from changes due to the solar flux and seasonal variations, we developed local empirical models of TEC and NmF2. These models were developed for November-March periods and selected locations. A TEC model now exists for a single longitude, 75^{o}W, and NmF2 models have been developed for several locations (Millstone Hill, 42.6^{o}N, 71.5^{o}W; Ramey, 18.5^{o}N, 67.1^{o}W; Jicamarca, 12.0^{o}S, 76.8^{o}W, and Port Stanley, 51.6^{o}S, 57.9^{o}W). Future effort will extend these models to a full year coverage.
2. We report a strong decrease in the electron density during SSW events in the nighttime and pre-sunrise ionosphere. This phenomenon is observed in the latitude range from ~55^{o}S to ~45^{o}N, with TEC decreasing to 20-25% of expected value (decrease by a up to a factor of 4-5) near 40^{o} S. Nighttime TEC is reduced by a factor of 2 at the equator.
3. At low latitudes, digisonde data indicate Spread-F development on such nights and in the areas of TEC decreases.
4. Particularly dramatic changes are observed around local sunrise at higher latitudes and include a sharp decrease in *Ne*, strong downward drifts (> 80m/s), and 100-300K decreases in ion temperature.
5. These features indicate that the nighttime ionosphere is strongly modified during SSW events. Some of these features are consistent with an enhancement in the thermospheric zonal wind, which presents an additional anomaly that is not well studied yet.

Acknowledgments and Data

Millstone Hill operations and research at MIT Haystack Observatory are supported by cooperative agreement AGS-1242204 between the US National Science Foundation and the Massachusetts Institute of Technology. L. Goncharenko was also supported through NSF grant AGS-1132267 and NASA LWS grant NNX13AI62G. M. Spraggs was supported by NSF REU grant during the summer 2014 REU project. A. Hernández-Espiet was supported by AGMUS Institute of Mathematics, Caribbean Computer Center for Excellence Alliance during his summer 2014 internship at the Haystack Observatory. We thank the operators of the Digisondes at Millstone Hill (USA), Ramey (Puerto Rico), Jicamarca (Peru), and Port Stanley (UK) for sharing their data through http://giro.uml.edu/. GPS TEC, Millstone Hill ISR, and Arecibo ISR data are publicly available through the Madrigal database at http://madrigal.haystack.mit.edu/madrigal/.

Figure Captions

Figure 1. A snapshot of a GPS TEC map at 17 UT on Jan 23, 2012 in the American longitudinal sector. Red stars show locations of other instruments: collocated incoherent scatter radars and

ionosondes: Millstone Hill, Arecibo (Ramey ionosonde), Jicamarca, as well as Port Stanley ionosonde.

Figure 2. Seasonal and diurnal variation in NmF2 as observed for $120 < F10.7 < 140$ (left) and predicted for F10.7 = 130 by empirical models for (top to bottom): Millstone Hill, Ramey, Jicamarca, and Port Stanley.

Figure 3. Performance of *NmF2* models in terms of MAPE (Mean Average Percentage Error, left) and Root Mean Square Error (RMSE, right) from November through March as function of universal time.

Figure 4. Latitudinal variations of total electron content at 75^{o}W and 8 UT (3 LT) as measured by GPS (color lines) and predicted by the empirical model. Thick dash lines show 25^{th} and 75^{th} percentiles of all TEC values observed within 7.5 degrees from 75^{o}W, for a range of F10.7=119-135 and from mid-December to mid-February. Thin dash lines show 10^{th} and 90^{th} percentiles, respectively.

Figure 5. The data to model ratio for GPS TEC at 75^{o}W on Jan 16, 2013, after the peak in stratospheric warming. Deep TEC depletion is observed throughout the local night hours (6-11 UT, 1-6 LT), with maximum TEC decrease occurring deeper and earlier in the Southern Hemisphere. This decrease is extended from ~55^{o}S to ~40^{o}N, with maximum TEC depletion by a factor of 4-5 at 40^{o}S.

Figure 6. Peak electron density NmF2 observed by different ionosondes during sudden stratospheric warming of 2013 in comparison with empirical NmF2 at the same locations. Lower than expected NmF2 is observed for several nights at all locations. Especially large NmF2 decrease is seen on Jan 18, 2013. Low-latitude F-region becomes strongly disturbed, with Spread-F development between 8-11 UT.

Figure 7. Ionospheric parameters Ne, Te, Ti, Vi (positive up) at mid-latitude as predicted by empirical model and observed by Millstone Hill ISR. Black line indicates the time of local sunrise at ionospheric altitudes. Sharp deep decrease in Ne develops on January 18, 2013 before the local sunrise, together with a ~300K cooling of Ti and a downward plasma motion.

Figure 8. Same as Figure 7, but for Arecibo ISR. Pre-sunrise decrease in Ne is accompanied by dramatic changes in Te, Ti, and Vi. Note that Ne decrease is observed ~1-1.5 hours earlier at Arecibo. Ti cooling is observed at higher altitudes (> 250 km) at both locations, but it is much smaller over Arecibo than over Millstone Hill.

Figure 9. TEC data/model ratio on January 28, 2008 (left) and January 14, 2012 (right), during minor SSW events. A broad area of decreased TEC develops from mid-latitudes in the Southern Hemisphere to tropical latitudes in the Northern Hemisphere and persists for multiple days.

Figure 10. NmF2 observations by Jicamarca ionosonde at nighttime (left) and daytime (right) for several days in January 2008. Ionosphere is strongly disturbed during both daytime and nighttime, with Spread-F development between 4 and 10 UT for several consecutive nights.

References

Araujo-Pradere, E. A., T. J. Fuller-Rowell, and M. V. Codrescu, STORM: An empirical storm-time ionospheric correction model, 1, Model description, Radio Sci., 37(5), 1070, doi:10.1029/2001RS002467, 2002.

Bailey, G.J., Sellek, R., Balan, N., 1991. The effect of interhemispheric coupling on nighttime enhancements in ionospheric total electron content during winter at solar minimum. Annales Geophysicae 9, 738–747.

Chau, J. L., B. G. Fejer, and L. P. Goncharenko (2009), Quiet variability of equatorial ExB drifts during a sudden stratospheric warming event, Geophys. Res. Lett., 36, L05101, doi:10.1029/2008GL036785.

Chau, J. L., N. A. Aponte, E. Cabassa, M. P. Sulzer, L. P. Goncharenko, and S. A. Gonzalez (2010), Quiet time ionospheric variability over Arecibo during sudden stratospheric warming events, J. Geophys. Res., 115, A00G06, doi:10.1029/2010JA015378.

Chau, J. L., L. P. Goncharenko, B. G. Fejer & H.-L. Liu (2012), Equatorial and low latitude ionospheric effects during sudden stratospheric warming events. Space Sci. Rev. 168: 385 - 417. doi:10.1007/s11214-011-9797-5.

Chen, Y., L. Liu, H. Le, W. Wan, and H. Zhang (2015), NmF2 enhancement during ionospheric F2 region nighttime: A statistical analysis based on COSMIC observations during the 2007–2009 solar minimum, J. Geophys. Res. Space Physics, 120, 10,083–10,095, doi:10.1002/2015JA021652.

de Jesus, R., I.S. Batista, P.R. Fagundes, K. Venkatesh, and A.J. de Abreu (2017), Ionospheric response to the 2006 sudden stratospheric warming event over the equatorial and low latitudes in the Brazilian sector using GPS observations, Journal of Atmospheric and Solar-Terrestrial Physics, Volume 154, February 2017, Pages 92-103, ISSN 1364-6826, http://dx.doi.org/10.1016/j.jastp.2016.12.005.

de Paula, E. R., O. F. Jonah, A. O. Moraes, E. A. Kherani, B. G. Fejer, M. A. Abdu, M. T. A. H. Muella, I. S. Batista, S. L. G. Dutra and R. R. Paes (2015), Low-latitude scintillation weakening during sudden stratospheric warming events, J. Geophys. Res. Space Physics, 120, DOI: 10.1002/2014JA020731.

Evans, J.V., 1965. Cause of the midlatitude winter night increase in foF2. Journal of Geophysical Research 70, 4331–4345.

Fagundes, P. R., L. P. Goncharenko, A. J. deAbreu, K. Venkatesh, M. Pezzopane, R. deJesus, M. Gende, AJ. Coster, and V. G. Pillat (2015), Ionospheric response to the 2009 sudden stratospheric warming over the equatorial, low- and mid-latitudes in the South American sector, J. Geophys. Res. Space Physics, 120, doi:10.1002/2014JA020649.

Farelo, A.F., Herraiz, M., Mikhailov, A.V., 2002. Global morphology of night-time NmF2 enhancements. Annales Geophysicae 20, 1795–1806.

Frissell, N. A., J. B. H. Baker, J. M. Ruohoniemi, R. A. Greenwald, A. J. Gerrard, E. S. Miller, and M. L. West (2016), Sources and characteristics of medium-scale traveling ionospheric disturbances observed by high-frequency radars in the North American sector, J. Geophys. Res. Space Physics, 121, 3722–3739, doi:10.1002/2015JA022168.

Fuller-Rowell, T., F. Wu, R. Akmaev, T.-W. Fang, and E. Araujo-Pradere (2010), A whole atmosphere model simulation of the impact of a sudden stratospheric warming on thermosphere dynamics and electrodynamics, J. Geophys. Res., 115, A00G08, doi:10.1029/2010JA015524.

Goncharenko, L. P., J. L. Chau, H.-L. Liu, and A. J. Coster (2010a), Unexpected Connections Between the Stratosphere and Ionosphere, Geophys. Res. Lett., 37, L10101, doi:10.1029/2010GL043125.

Goncharenko, L. P., A. J. Coster, J. L. Chau, and C. E. Valladares (2010b), Impact of sudden stratospheric warmings on equatorial ionization anomaly, J. Geophys. Res., 115, A00G07, doi:10.1029/2010JA015400.

Goncharenko, L., J. L. Chau, P. Condor, A. Coster, and L. Benkevitch (2013), Ionospheric effects of sudden stratospheric warming during moderate-to-high solar activity: Case study of January 2013, Geophys. Res. Lett., 40, doi:10.1002/grl.50980.

Jakowski, N., Forster, M., 1995. About the nature of the night-time winter anomaly effect (NWA) in the F-region of the ionosphere. Planetary and Space Science 43, 603–612.

Jonah, O. F., E. R. de Paula, E. A. Kherani, S. L. G. Dutra, and R. R. Paes (2014), Atmospheric and ionospheric response to sudden stratospheric warming of January 2013, J. Geophys. Res. Space Physics, 119, 4973–4980, doi:10.1002/2013JA019491.

Liu, H., Y. Miyoshi, S. Miyahara, H. Jin, H. Fujiwara, and H. Shinagawa (2014), Thermal and dynamical changes of the zonal mean state of the thermosphere during the 2009 SSW: GAIA simulations, J. Geophys. Res. Space Physics, 119, doi:10.1002/2014JA020222.

Maute, A., M. E. Hagan, V. Yudin, H.-L. Liu, and E. Yizengaw (2015), Causes of the longitudinal differences in the equatorial vertical $E \times B$ drift during the 2013 SSW period as simulated by the TIME-GCM, J. Geophys. Res. Space Physics, 120, doi: 10.1002/2015JA021126.

McDonald, S. E., F. Sassi, and A. J. Mannucci (2015), SAMI3/SD-WACCM-X simulations of ionospheric variability during northern winter 2009, Space Weather, 13, 568–584, doi:10.1002/2015SW001223.

Mikhailov, A.V., Forster, M., Leschinskaya, T.Y., 2000. On the mechanism of the post-midnight winter NmF2 enhance- ments: dependence on solar activity. Annales Geophysicae 18, 1422–1434.

Miyoshi, Y., H. Fujiwara, H. Jin, and H. Shinagawa (2015), Impacts of sudden stratospheric warming on general circulation of the thermosphere, J. Geophys. Res. Space Physics, 120, doi:10.1002/2015JA021894.

Pedatella, N. M. and J. M. Forbes (2010), Evidence for Stratosphere Sudden Warming-Ionosphere Coupling Due to Vertically Propagating Tides, Geophys. Res. Lett., 37, L11104, doi:10.1029/2010GL043560.

Pedatella, N. M., and H.-L. Liu (2013), The influence of atmospheric tide and planetary wave variability during sudden stratosphere warmings on the low latitude ionosphere, J. Geophys. Res. Space Physics, 118, doi:10.1002/jgra.50492.

Pedatella, N. M., H.-L. Liu, F. Sassi, J. Lei, J. L. Chau, and X. Zhang (2014), Ionosphere variability during the 2009 SSW: Influence of the lunar semidiurnal tide and mechanisms producing electron density variability, J. Geophys. Res. Space Physics, 119, 3828–3843, doi:10.1002/2014JA019849.

Pedatella, N. M., and A. Maute (2015), Impact of the semidiurnal lunar tide on the midlatitude thermospheric wind and ionosphere during sudden stratosphere warmings, J. Geophys. Res. Space Physics, 120, 10,740–10,753, doi:10.1002/2015JA021986.

Reinisch, B.W., I.A. Galkin, G.M. Khmyrov et al. (2009), The New Digisonde for Research and Monitoring Applications, *Radio Sci*., *44* RS0A24, doi:10.1029/2008RS004115.

Reinisch, B. W., and I. A. Galkin, Global ionospheric radio observatory (GIRO), Earth, Planets, and Space, 63, 377-381, doi:10.5047/eps.2011.03.001, 2011.

Rideout, W., and A. Coster (2006), Automated GPS processing for global total electron content data, GPS Solutions, doi:10.1007/s10291-006-0029-5.

Sumod, S. G., T.K. Pant, Lijo Jose, M.M.Hossain and K.K.Kumar (2012), Signatures of sudden stratospheric warming on the equatorial ionosphere-thermosphere system, *Planetary and SpaceScience*, doi:10.1016/j.pss.2011.08.005

Vieira, F., P. R. Fagundes, K. Venkatesh, L. P. Goncharenko, and V. G. Pillat (2017), Total electron content disturbances during minor sudden stratospheric warming, over the Brazilian region: A case study during January 2012, J. Geophys. Res. Space Physics, 122, 2119–2135, doi:10.1002/2016JA023650.

Zhang, S.-R., J. M. Holt, A. P. van Eyken, M. McCready, C. Amory-Mazaudier, S. Fukao, and M. Sulzer (2005), Ionospheric Local Model and Climatology from Long-Term Databases of Multiple Incoherent Scatter Radars, Geophys. Res. Lett., 32, L20102, doi:10.1029/2005GL023603.

Zhang, S.- R., J. C. Foster, A. J. Coster, and P. J. Erickson (2011), East-West Coast differences in total electron content over the continental US, Geophys. Res. Lett., 38, L19101, doi:10.1029/2011GL049116

Zhang, S.-R., J. C. Foster, J. M. Holt, P. J. Erickson, and A. J. Coster (2012), Magnetic declination and zonal wind effects on longitudinal differences of ionospheric electron density at midlatitudes, J. Geophys. Res., 117, A08329, doi:10.1029/2012JA017954.

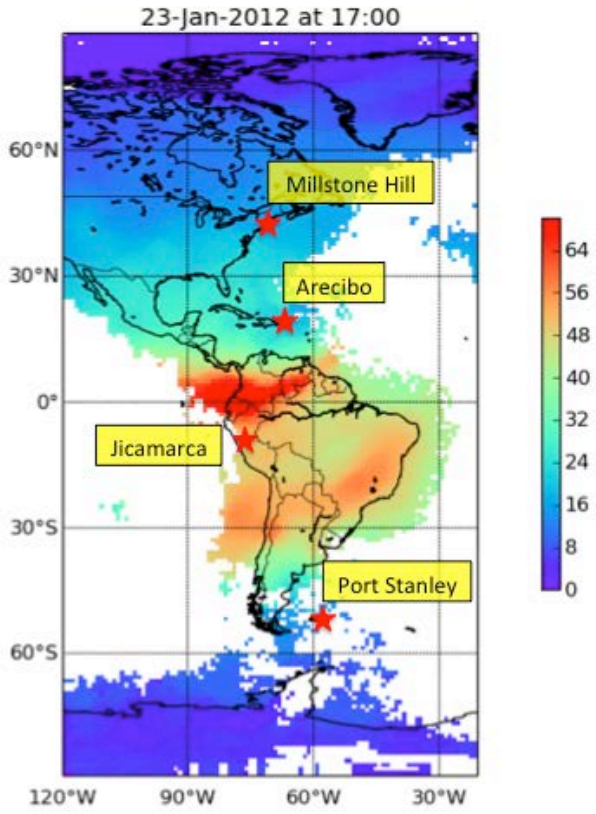

Figure 1. A snapshot of a GPS TEC map at 17 UT on Jan 23, 2012 in the American longitudinal sector. Red stars show locations of other instruments: co-located incoherent scatter radars and ionosondes at Millstone Hill, Arecibo (Ramey ionosonde), Jicamarca, and Port Stanley.

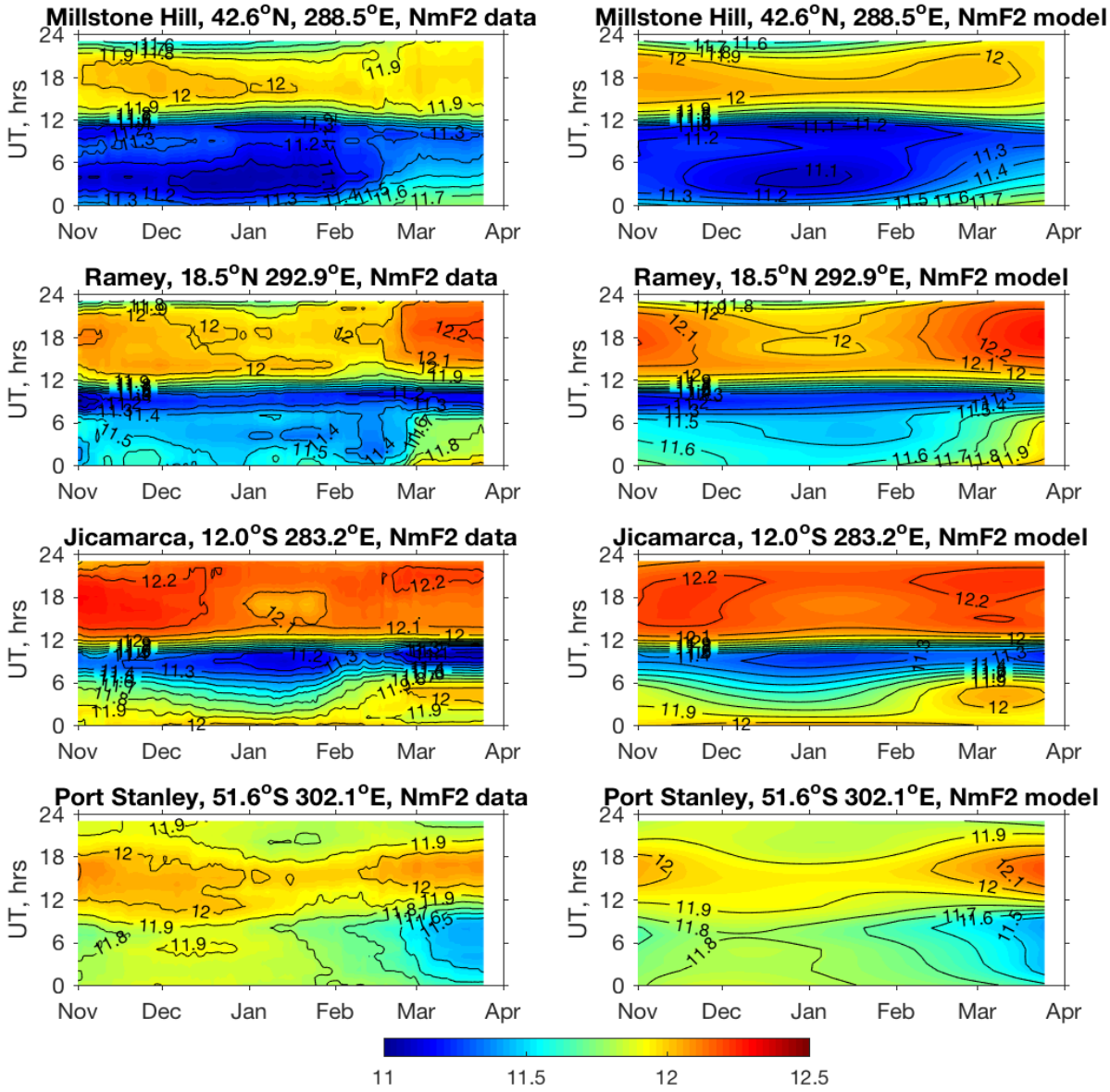

Figure 2. Seasonal and diurnal variation in NmF2 as observed for 120 < F10.7 < 140 (left) and predicted for F10.7 = 130 by empirical models for (top to bottom): Millstone Hill, Ramey, Jicamarca, and Port Stanley.

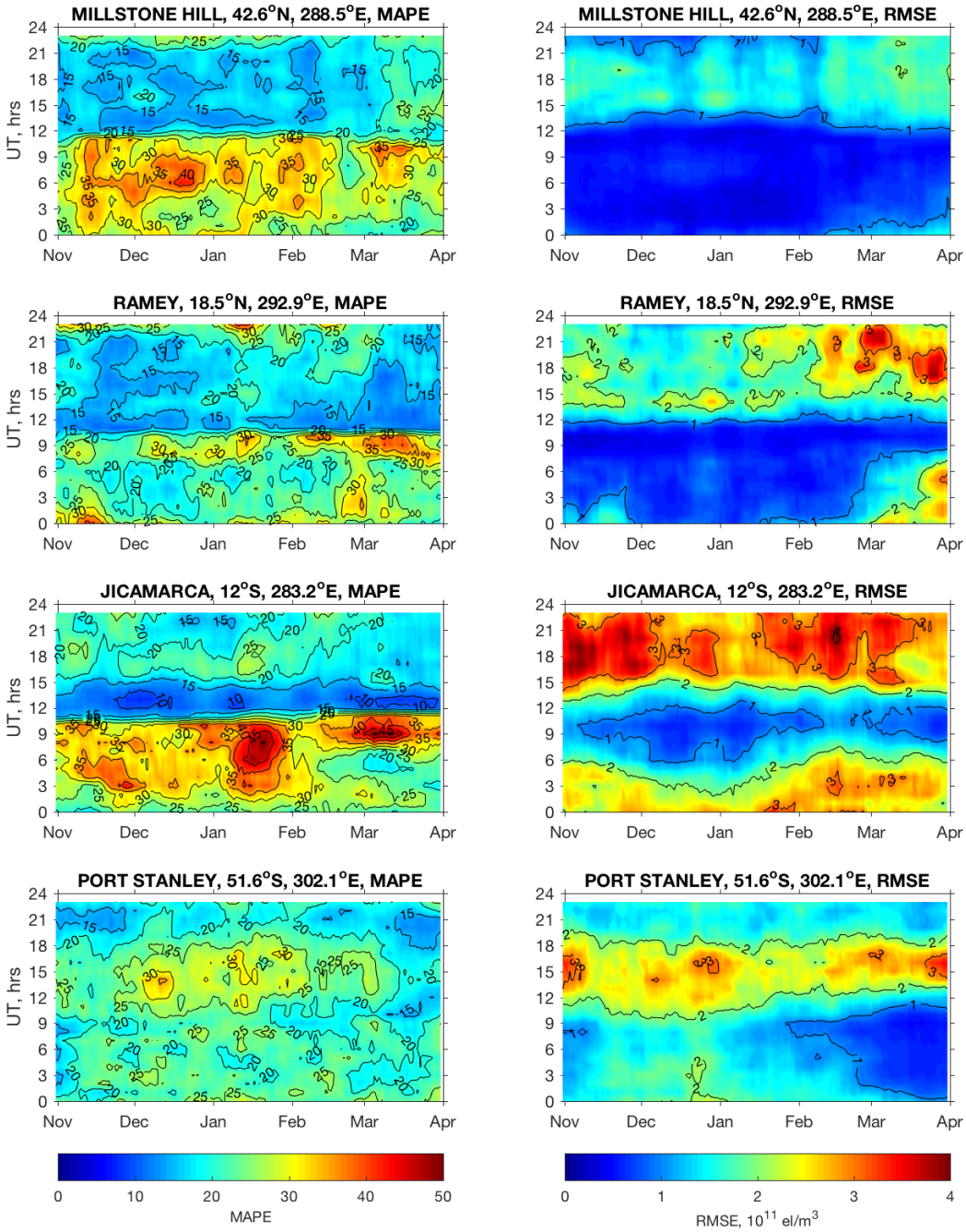

Figure 3. Performance of *NmF2* models in terms of MAPE (Mean Average Percentage Error, left) and Root Mean Square Error (RMSE, right) from November through March as function of universal time.

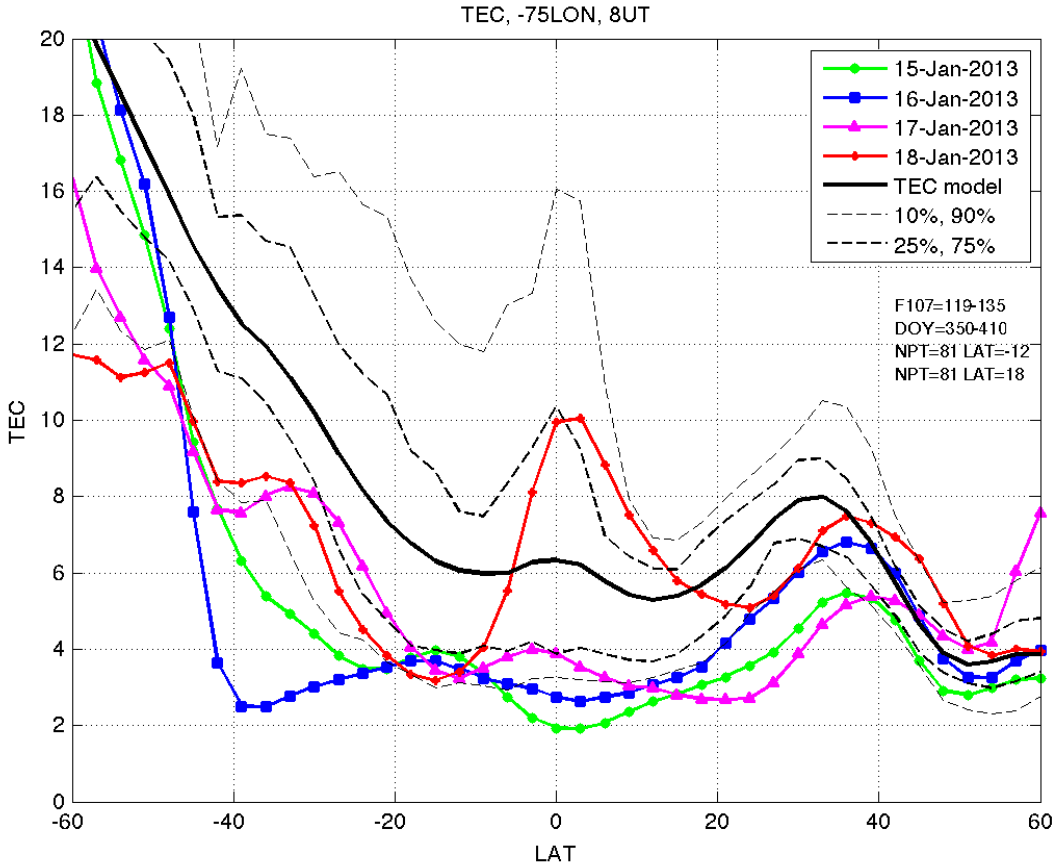

Figure 4. Latitudinal variations of total electron content at 75°W and 8 UT (3 LT) as measured by GPS (color lines) and predicted by the empirical model (solid black contour). Thick dash lines show the 25th and 75th percentiles of all TEC values observed within 7.5 degrees from 75°W, for a range of F10.7=119-135 and from mid-December to mid-February (DOY 350 – 410). Thin dash lines show the 10th and 90th percentiles, respectively.

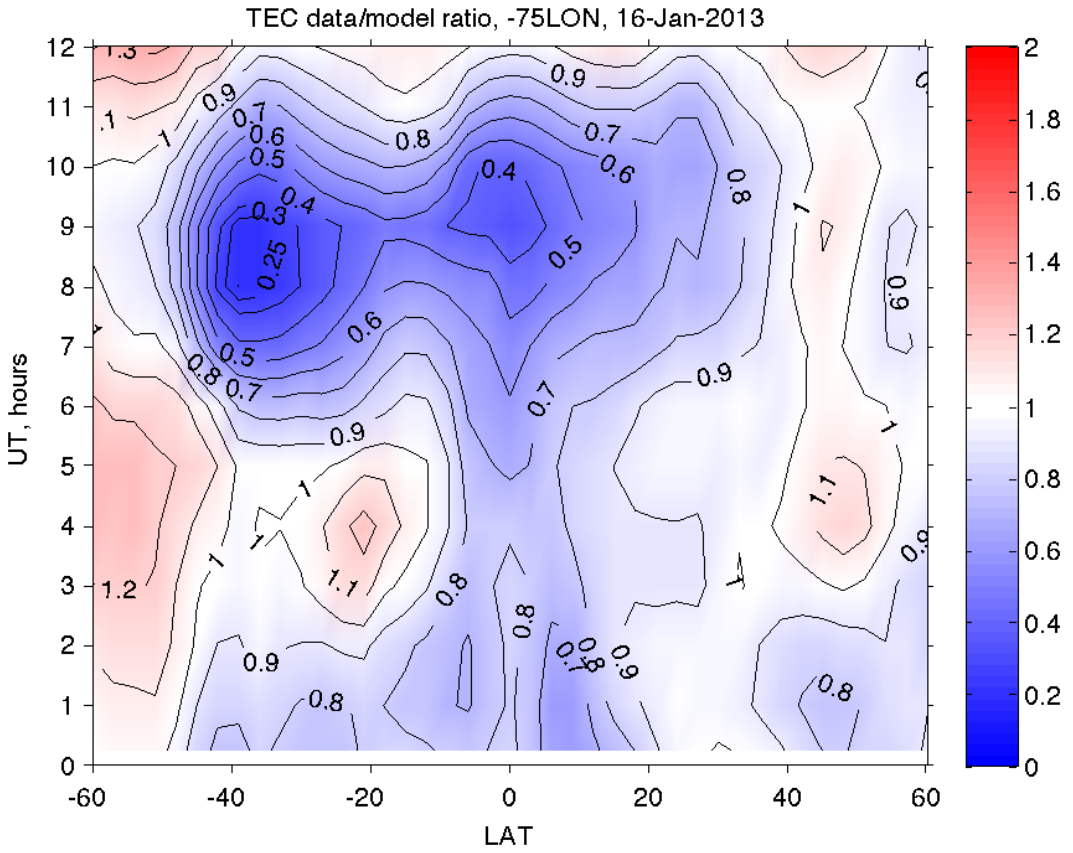

Figure 5. The data to model ratio for GPS TEC at 75°W on Jan 16, 2013, after the peak of the stratospheric warming. Deep TEC depletion is observed throughout the local night hours (6-11 UT, 1-6 LT), with maximum TEC decreases occurring deeper and earlier in the Southern Hemisphere. This decrease is extends from ~55°S to ~40°N, with maximum TEC depletion by a factor of 4-5 at 40°S.

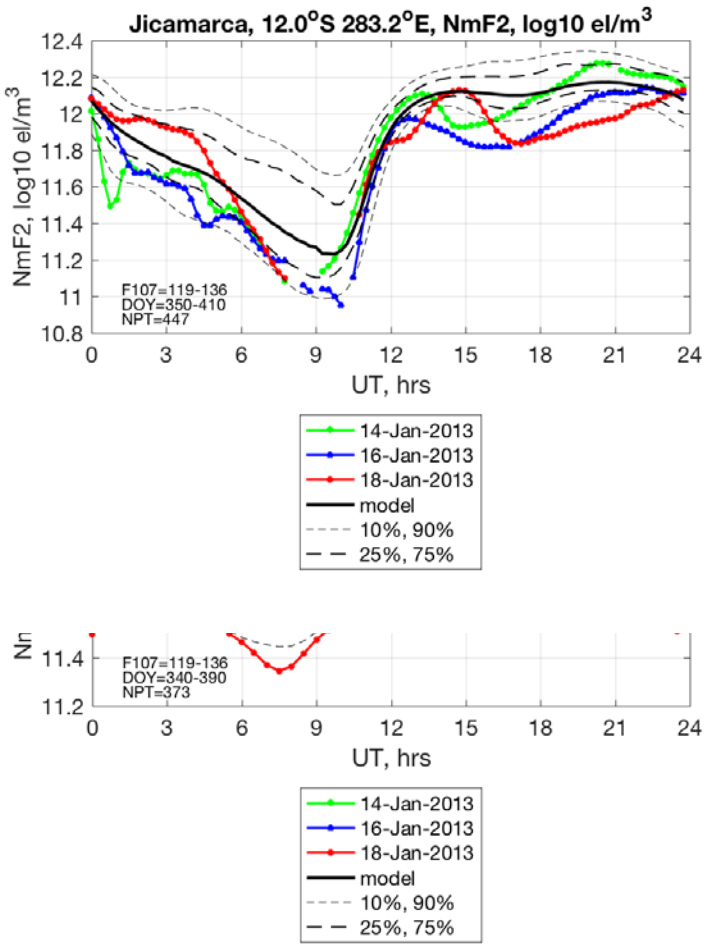

Figure 6. Peak electron density *NmF2* observed by different ionosondes during the sudden stratospheric warming of 2013 in comparison with empirical model *NmF2* at the same locations. Lower than expected *NmF2* is observed for several nights at all locations. An especially large *NmF2* decrease is seen on Jan 18, 2013. Low-latitude F-region becomes strongly disturbed, with Spread-F development between 8-11 UT.

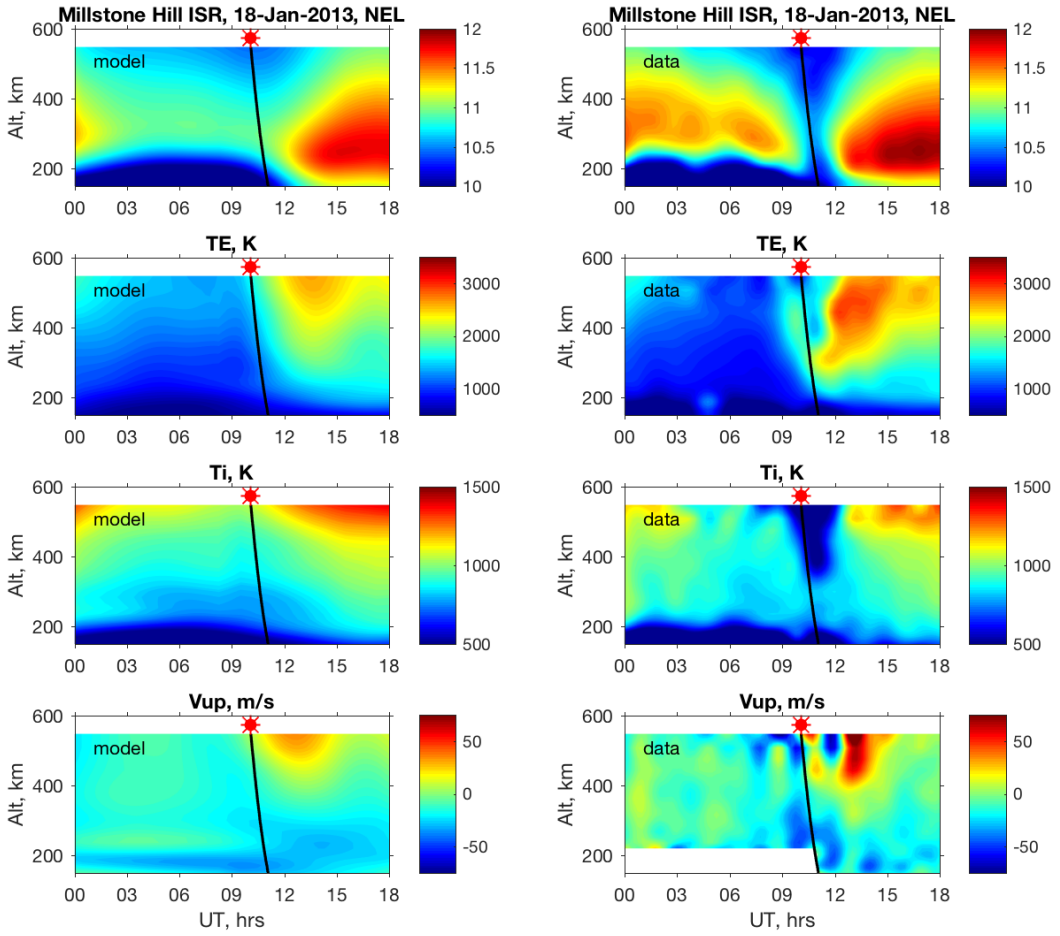

Figure 7. Ionospheric parameters *Ne*, *Te*, *Ti*, *Vi* (positive up) in mid-latitudes as predicted by the empirical model (left) and observed by Millstone Hill ISR (right). Black line indicates the time of local sunrise at ionospheric altitudes. Sharp deep decrease in *Ne* develops on January 18, 2013 before the local sunrise, together with a ~300K cooling of *Ti* and a downward plasma motion.

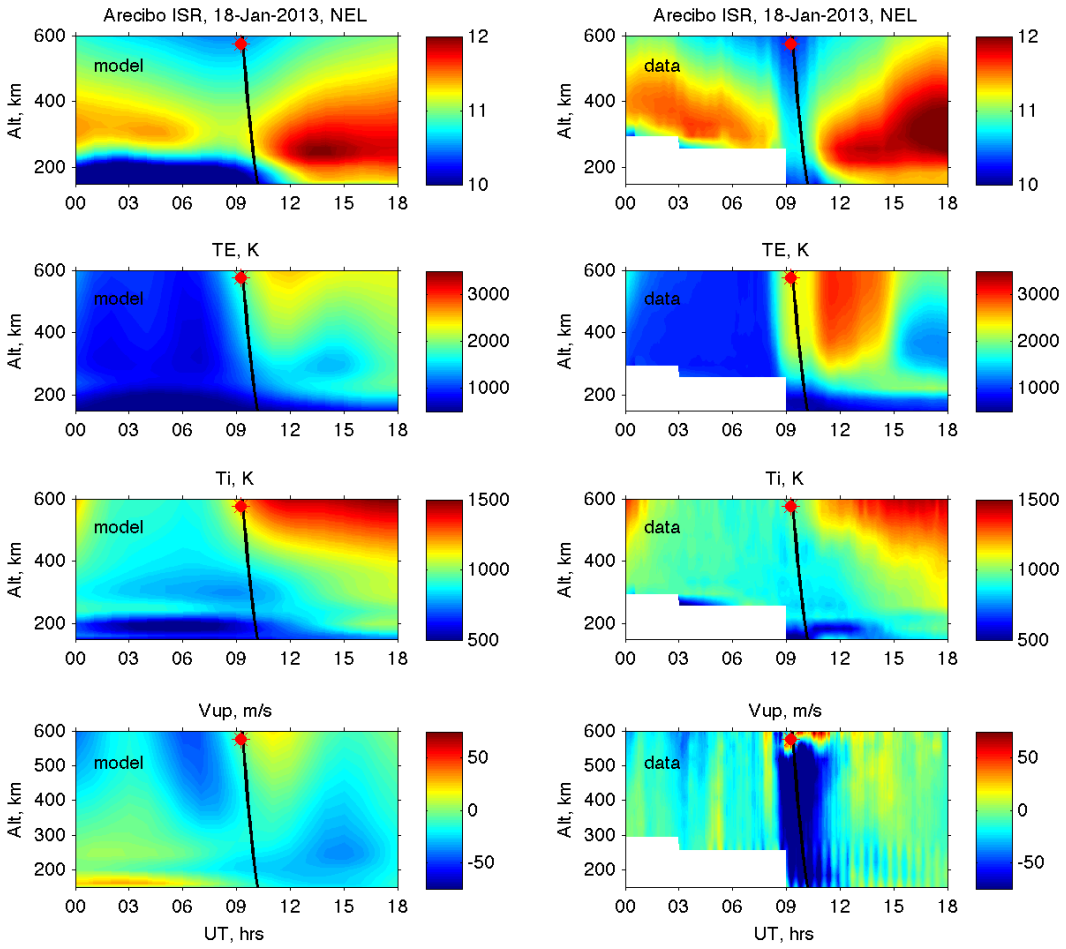

Figure 8. Same as Figure 7, but for the Arecibo ISR. Pre-sunrise decreases in *Ne* are accompanied by dramatic changes in *Te*, *Ti*, and *Vi*. Note that *Ne* decrease is observed ~1-1.5 hours earlier at Arecibo. *Ti* cooling is observed at higher altitudes (> 250 km) at both locations, but it is much smaller over Arecibo than over Millstone Hill.

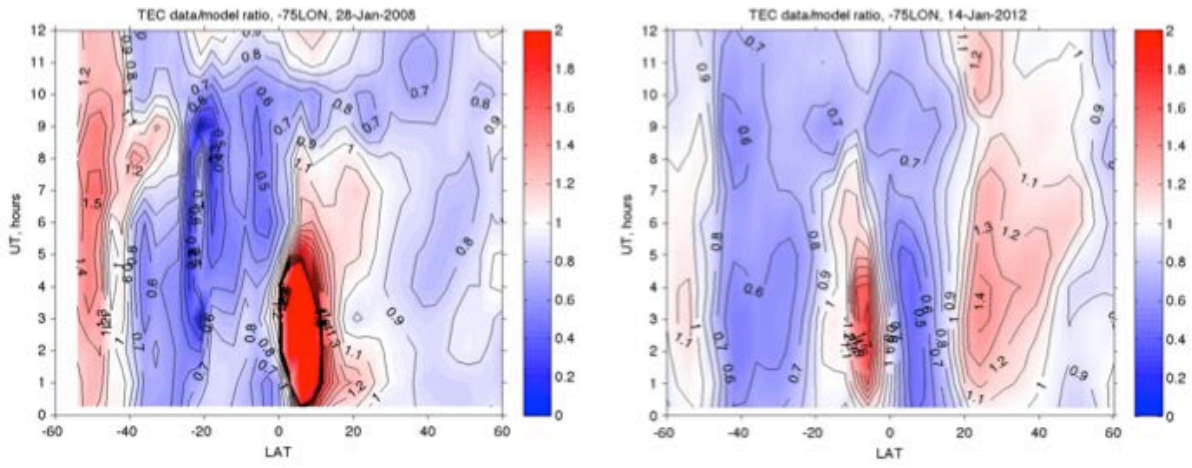

Figure 9. TEC data/model ratio on January 28, 2008 (left) and January 14, 2012 (right), during minor SSW events. A broad area of decreased TEC develops from mid-latitudes in the Southern Hemisphere to tropical latitudes in the Northern Hemisphere and persists for multiple days.

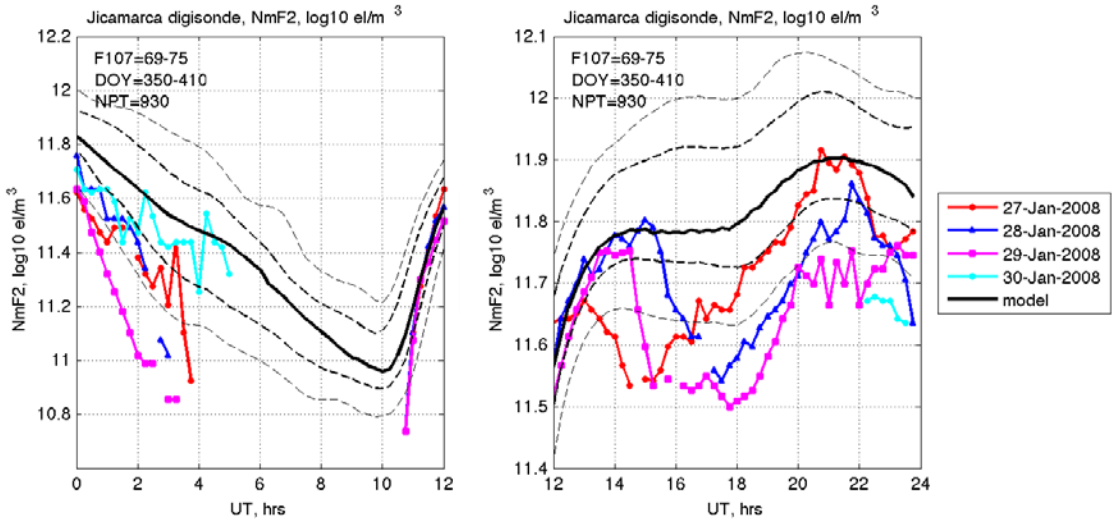

Figure 10. *NmF2* observations by the Jicamarca ionosonde during the nighttime (left) and daytime (right) for several days in January 2008. Ionosphere is strongly disturbed during both daytime and nighttime, with Spread-F development between 4 and 10 UT for several consecutive nights.

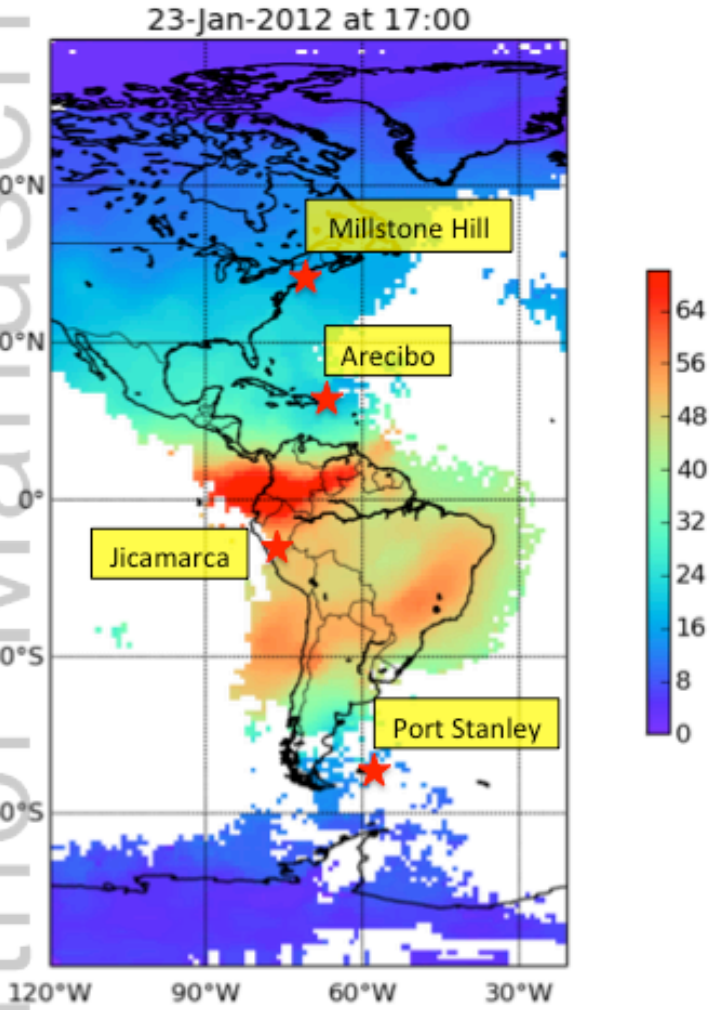

2018JA025541-f01-z-.png

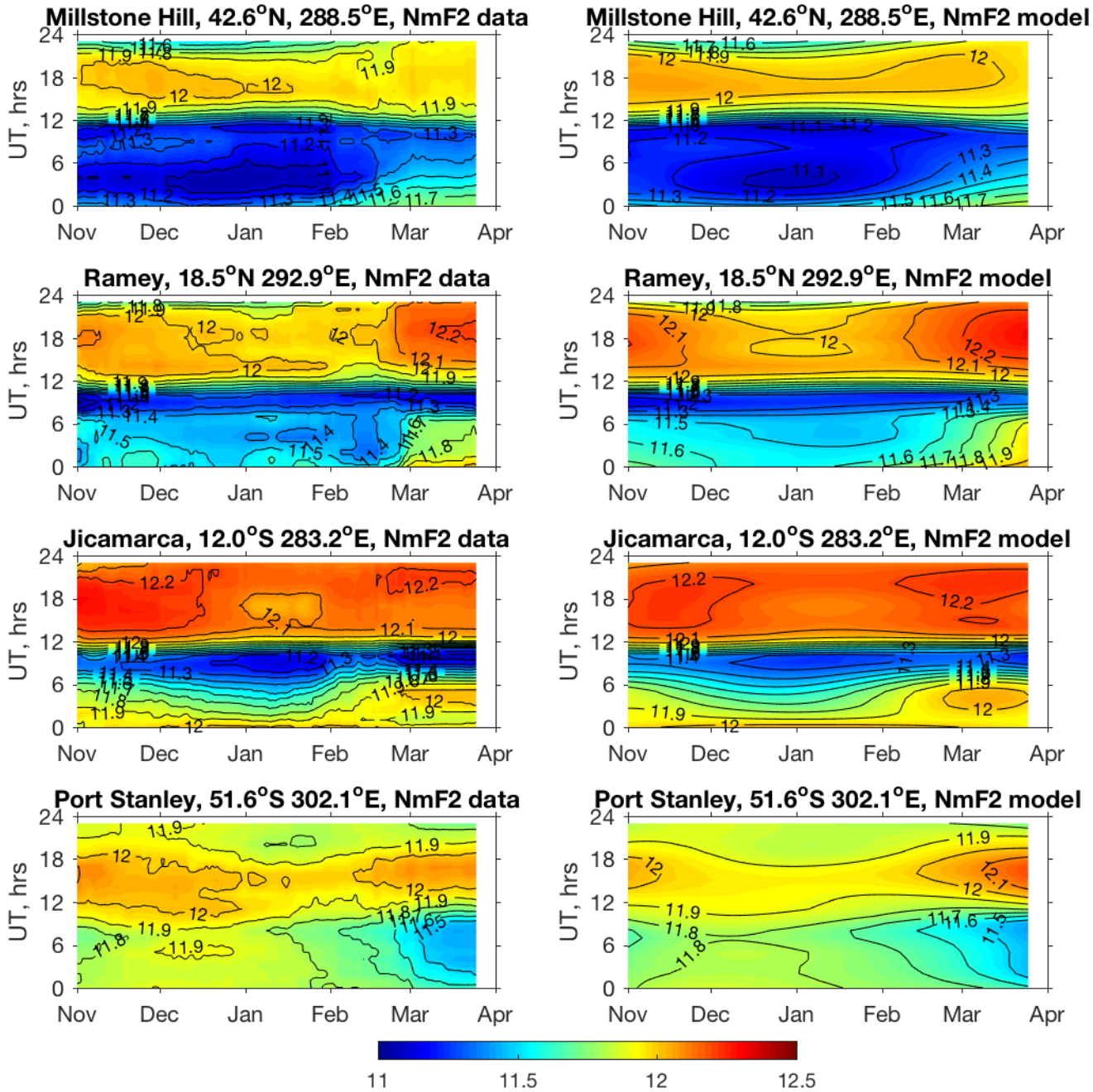

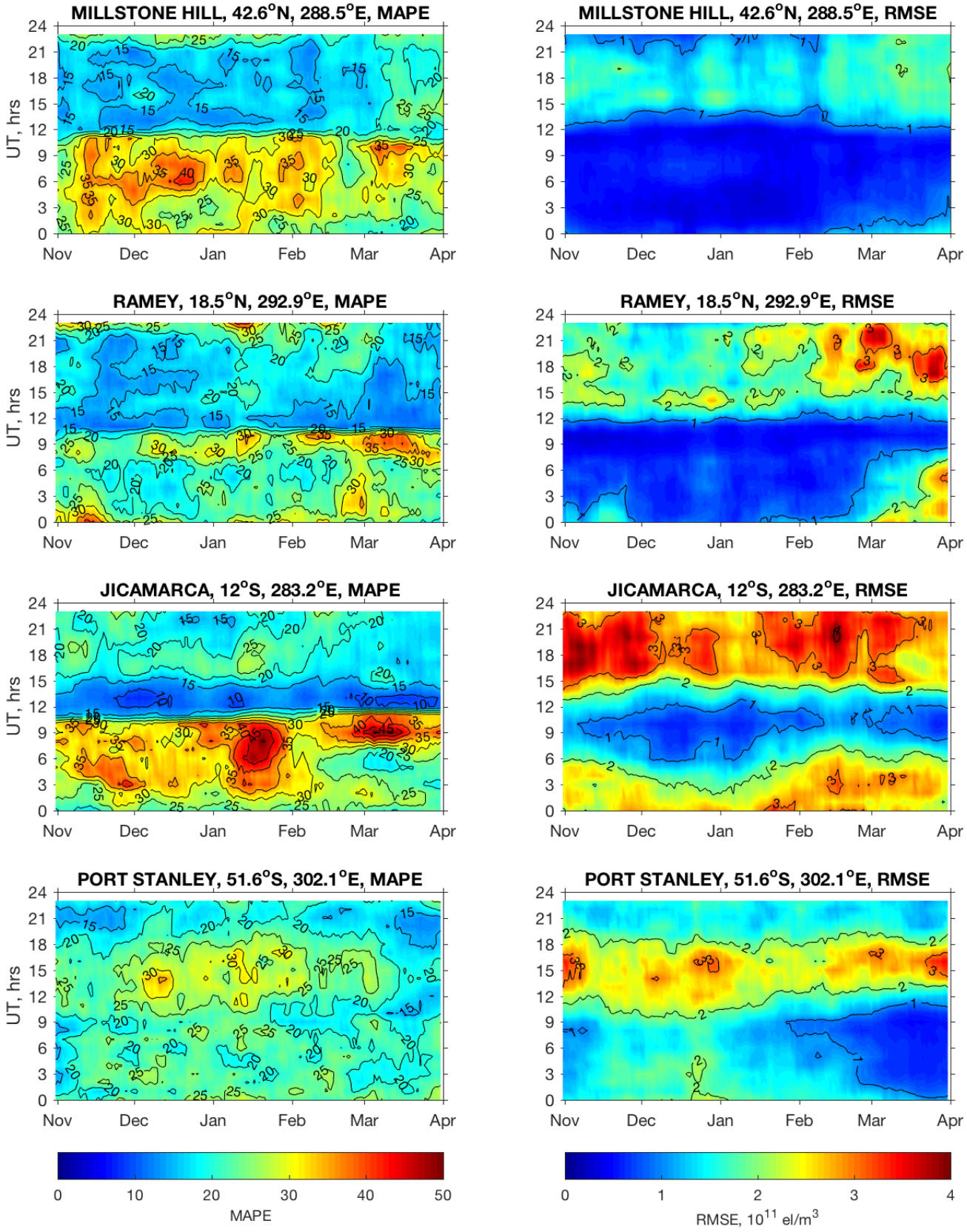

2018JA025541-f03-z-.png

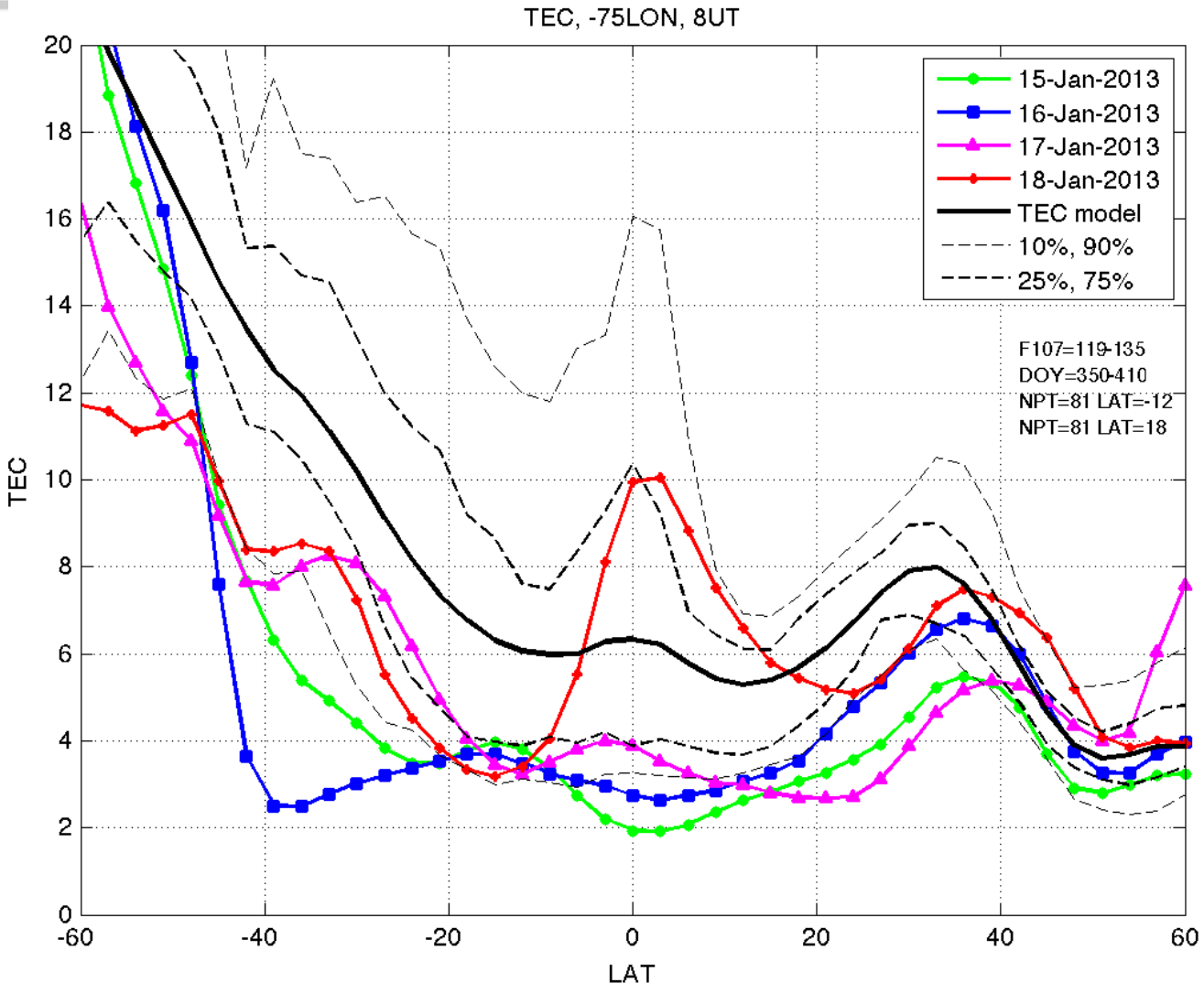

2018JA025541-f04-z-.png

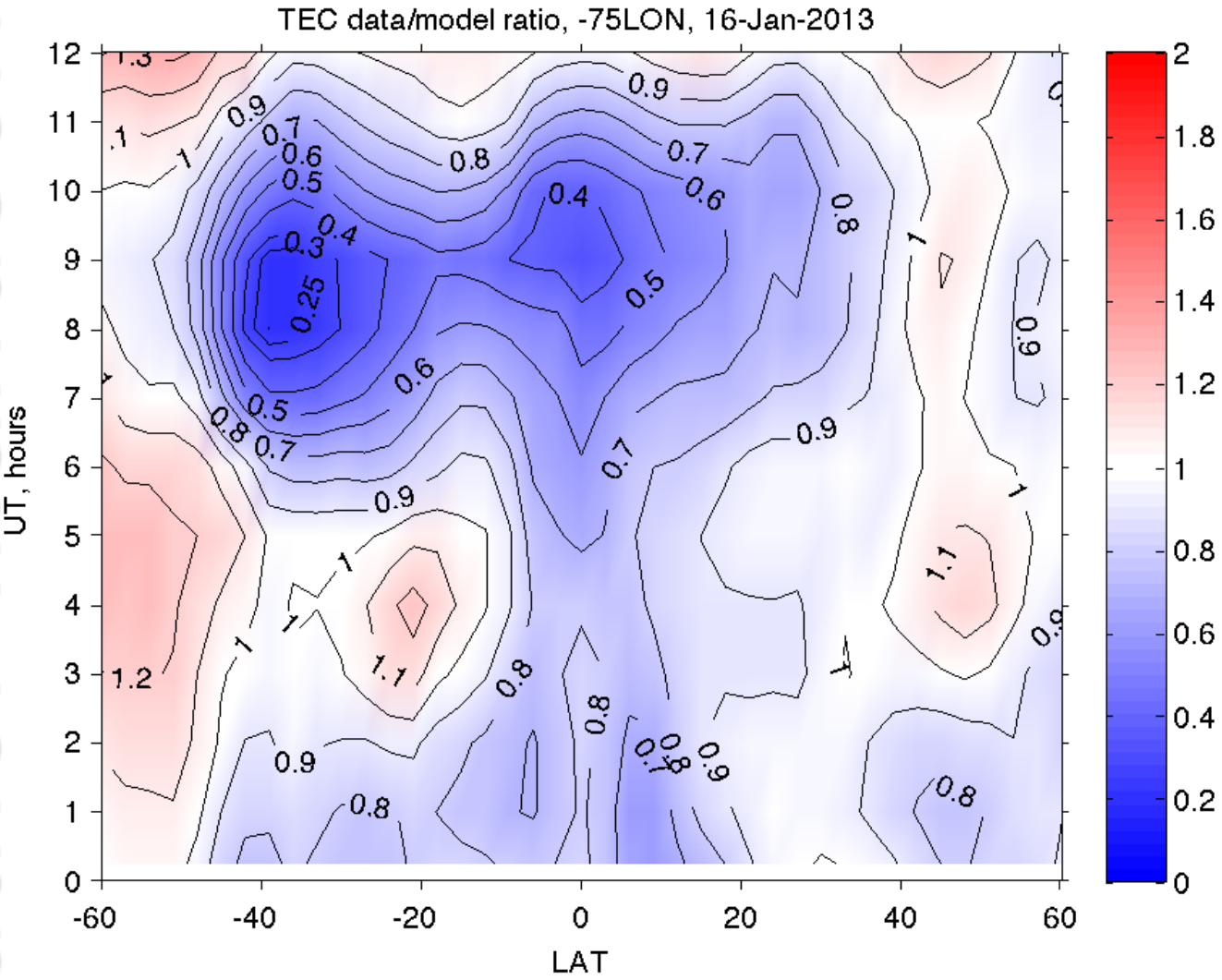

2018JA025541-f05-z-.png

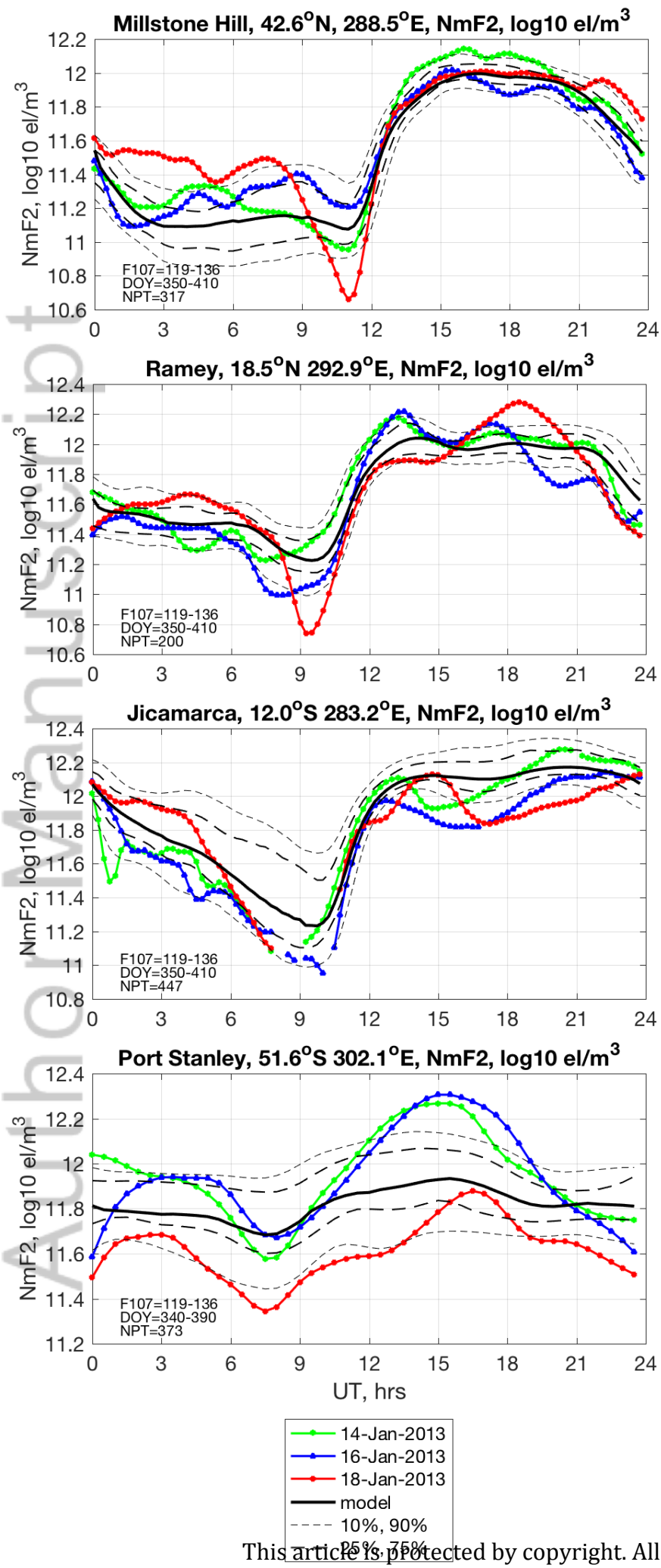

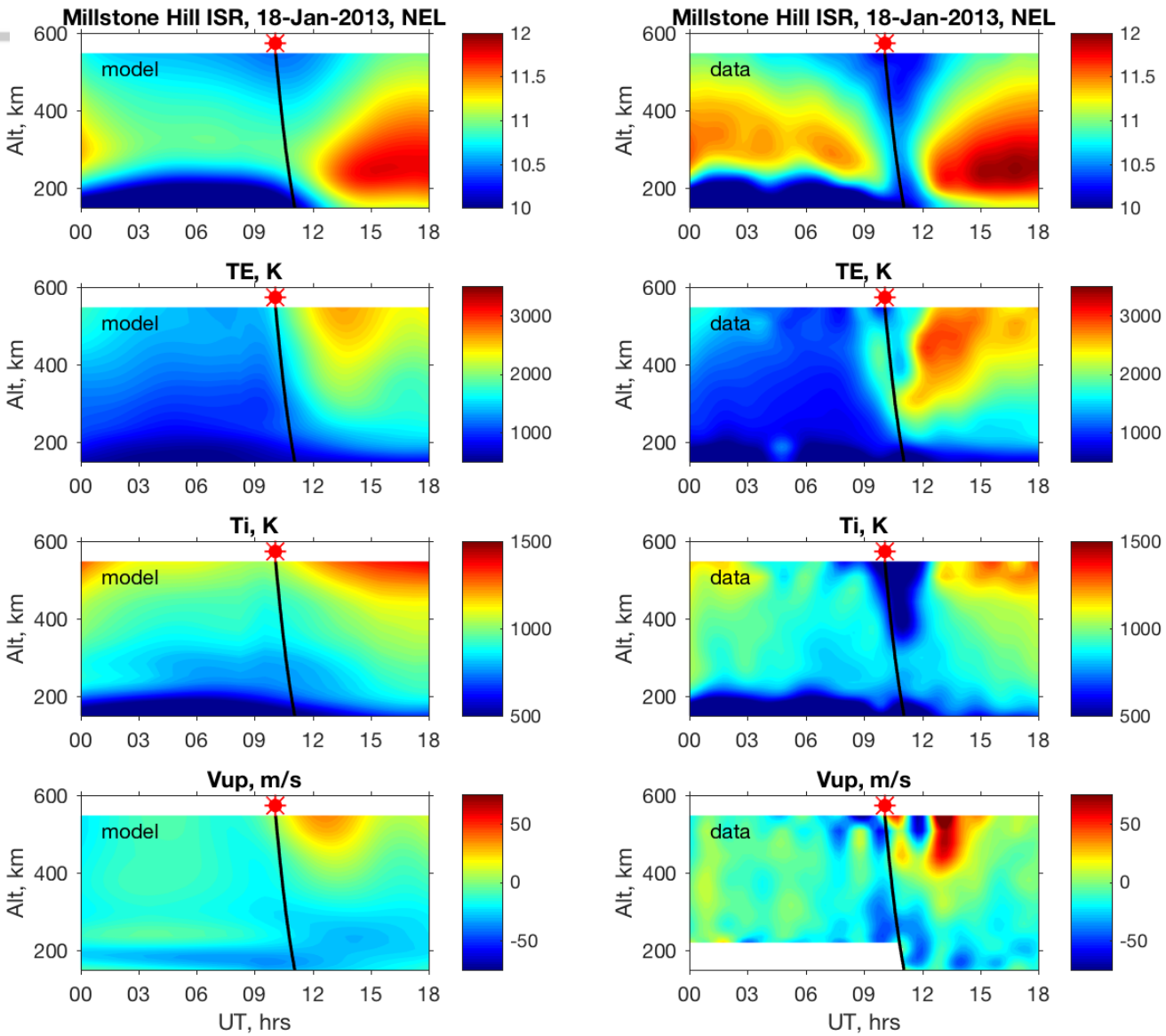

2018JA025541-f07-z-.png

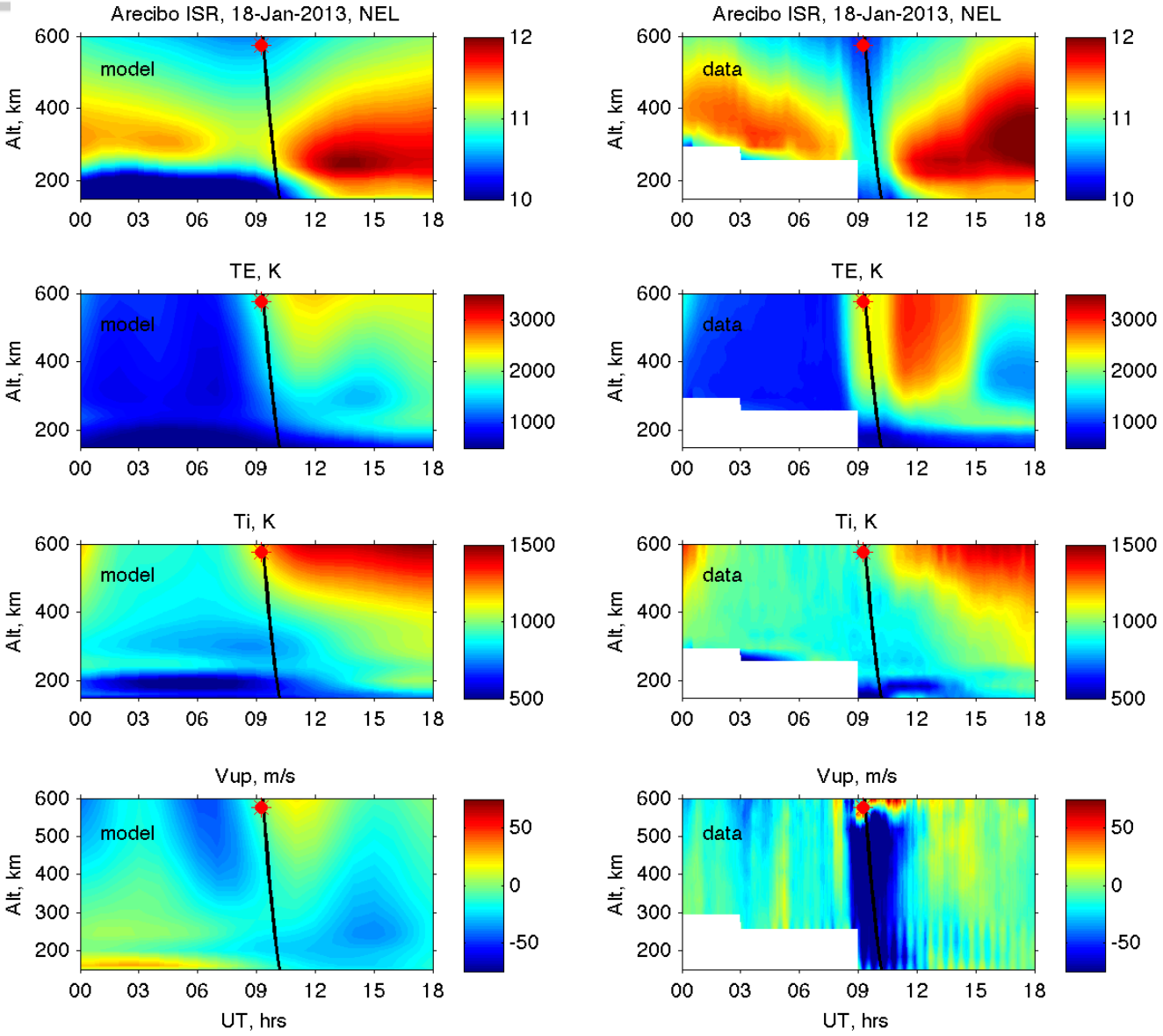

2018JA025541-f08-z-.png

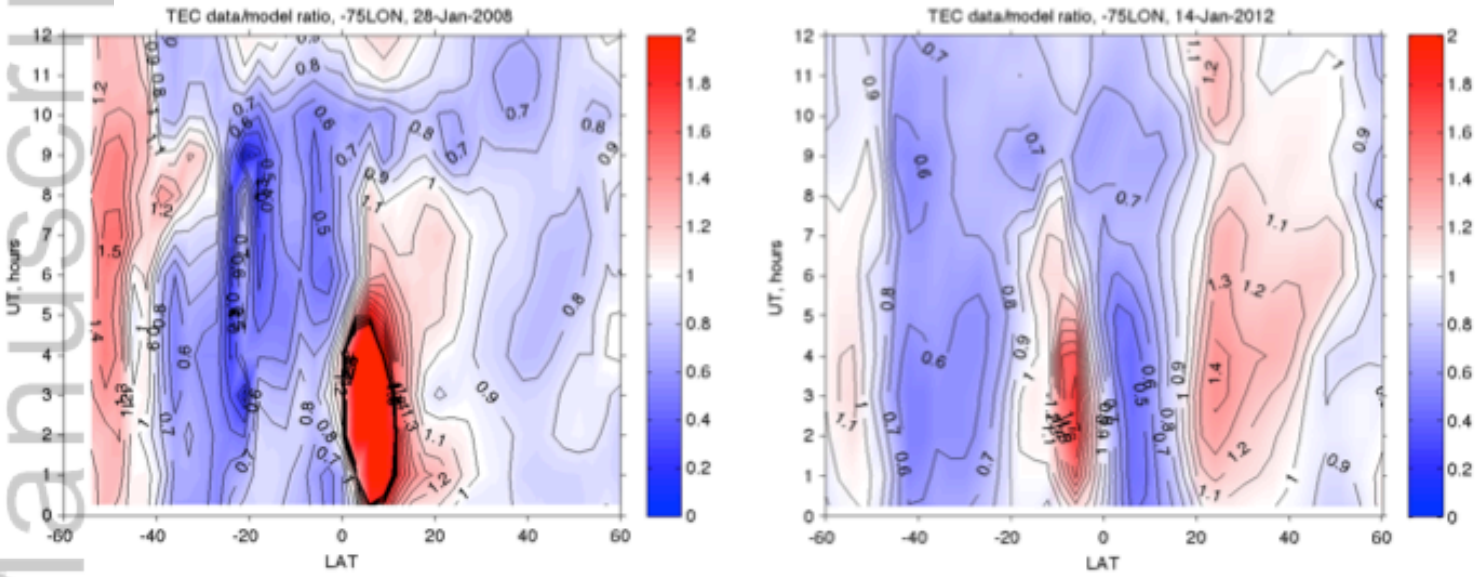

2018JA025541-f09-z-.png